UNIVERSITY OF THESSALY
MECHANICAL AND INDUSTRIAL ENGINEERING DEPARTMENT

CRACK IDENTIFICATION IN STRUCTURES USING OPTIMAL SENSOR LOCATIONS

By

GAITANAROS STAVROS

Diploma in Mechanical & Industrial Engineering, University of Thessaly 2005

A Thesis
Submitted in Partial Fulfillment of the
Requirements for the Degree of
Master of Science
(in Mechanical & Industrial Engineering)

2007

ΠΑΝΕΠΙΣΤΗΜΙΟ ΘΕΣΣΑΛΙΑΣ
ΠΟΛΥΤΕΧΝΙΚΗ ΣΧΟΛΗ
ΤΜΗΜΑ ΜΗΧΑΝΟΛΟΓΩΝ ΜΗΧΑΝΙΚΩΝ ΒΙΟΜΗΧΑΝΙΑΣ

Μεταπτυχιακή Εργασία

ΑΝΑΓΝΩΡΙΣΗ ΡΩΓΜΩΝ ΣΕ ΚΑΤΑΣΚΕΥΕΣ ΜΕ ΒΕΛΤΙΣΤΗ ΤΟΠΟΘΕΤΗΣΗ ΑΙΣΘΗΤΗΡΩΝ

υπό

ΣΤΑΥΡΟΥ ΓΑΪΤΑΝΑΡΟΥ

Διπλωματούχου Μηχανολόγου Μηχανικού Βιομηχανίας Π.Θ, 2005

Υπεβλήθη για την εκπλήρωση μέρους των
απαιτήσεων για την απόκτηση του
Μεταπτυχιακού Διπλώματος Ειδίκευσης
2007

Εγκρίθηκε από τα Μέλη της Πενταμελούς Εξεταστικής Επιτροπής:

Πρώτος Εξεταστής (Επιβλέπων)	Δρ. Κωνσταντίνος Παπαδημητρίου Καθηγητής, Τμήμα Μηχανολόγων Μηχανικών Βιομηχανίας, Πανεπιστήμιο Θεσσαλίας
Δεύτερος Εξεταστής	Δρ. Νικόλαος Αράβας Καθηγητής, Τμήμα Μηχανολόγων Μηχανικών Βιομηχανίας, Πανεπιστήμιο Θεσσαλίας
Τρίτος Εξεταστής	Δρ. Σπύρος Καραμάνος Επίκουρος Καθηγητής, Τμήμα Μηχανολόγων Μηχανικών Βιομηχανίας, Πανεπιστήμιο Θεσσαλίας
Τέταρτος Εξεταστής	Δρ. Αναστάσιος Σταμάτης Επίκουρος Καθηγητής, Τμήμα Μηχανολόγων Μηχανικών Βιομηχανίας, Πανεπιστήμιο Θεσσαλίας
Πέμπτος Εξεταστής	Δρ. Γεώργιος Πετρόπουλος Επίκουρος Καθηγητής, Τμήμα Μηχανολόγων Μηχανικών Βιομηχανίας, Πανεπιστήμιο Θεσσαλίας

Acknowledgements

At this point I would like to express my sincerest gratitude to my academic advisor, Professor Costas Papadimitriou for the guidance during all the years he was my advisor. Working close to him was an invaluable experience, a motive to always give my best, and one of the main reasons that made me pursue graduate studies.

I would also like to thank Professor N. Aravas for his contribution in this thesis with his important remarks and advices in topics of Fracture Mechanics. My specific gratitude to Professor Spyros Karamanos whose personal interest during the last three years made him substantially a co-advisor for me.

Special attribute must be given to my colleague and PhD candidate G. Karaiskos cause this work was a result of an effective collaboration with him. His contribution to specific topics as the finite element modeling but mainly to most problems that arose during the preparation of this thesis is highly appreciated. A very large thank you to all guys in the lab for the quality time we spent together in and out of the university.

I would like to thank my two sisters for their love and support. My mother for her trust in my capabilities that urged me to become who I am today and her continuous support regardless of her opinion on my choices. The feeling of safety and freedom that she always offered me often kept me focused to my plans despite all obstacles.

Finally, I dedicate this thesis to the one person with whom I shared all my thoughts and worries for the past 6 years.

to my partner and closest friend

Maria

CRACK IDENTIFICATION IN STRUCTURES USING OPTIMAL SENSOR LOCATIONS

Abstract

A Bayesian system identification methodology is presented for estimating the crack location, size and orientation using strain measurements. The Bayesian statistical approach combines information from measured data and analytical or computational models of structural behavior to predict estimates of the crack characteristics along with the associated uncertainties, taking into account modeling and measurement errors. An optimal sensor location methodology is proposed to maximize the information that is contained in the measured data for crack identification problems. For this, the most informative, about the condition of the structure, data are obtained by minimizing the information entropy measure of the uncertainty in the model parameter estimates provided by the above statistical system identification method. Both crack identification and optimal sensor location formulations lead to highly non-convex optimization problems in which multiple local and global optima may exist. A hybrid optimization method based on evolutionary strategies and gradient based techniques is used to determine the global minimum. The effectiveness of the proposed methodologies is illustrated using simulated data from a single crack in a thin plate subjected to known and unknown static loading. The effects of modeling and measurement error on the effectiveness of the crack detection method, as well as the methodology's limitations are investigated.

Contents

CHAPTER 1

INTRODUCTION

The problem of crack detection in structures has received much attention over the years because of its profound importance in structural health monitoring. Early detection of cracks is a key element for preventing catastrophic failure and prolonging the life of structures. Crack identification information can be used for developing cost-effective maintenance procedures for structures, improving their safety and reducing their maintenance and rehabilitation costs, in a whole-life cost basis. Current inspection techniques, based on vibration analysis and wave propagation, involve complex, time-consuming procedures, which can be very labor-intensive and expensive. Therefore, a fast, low cost built-in structural health monitoring system involving a sensor array along with fast processing techniques is needed to overcome the shortcomings of the current inspection techniques.

Damage detection is generally approached by several techniques. One category of them is based on the changes in the global vibrational properties of a structure caused by damage [1-6]. However, this approach is only effective in dealing with larger defects for the obvious reason that the effects of small flaws on the global vibrational properties are often below the noise level in large structures. Other techniques use changes in the characteristics of ultrasonic waves propagating across existing defects [7-10]. Ultrasonic approaches, although highly effective in detecting very small defects, require a dense network of sensors that is impractical to implement in larger structures and raises significantly the cost of the equipment. Techniques based on strain measurements from

optical fibers for identifying cracks have also been pursued experimentally [11-13]. Based on the experimental results, this method has been shown to be promising for detecting cracks. Limited studies have shown that the method effectiveness depends on the location and number of sensors with respect to the crack. Other limitations of the current defects detection methodologies are the presence of ambient noise and more importantly the need for manual analysis of the signals resulting in extremely time-consuming inspection procedures and strong operator-dependent conclusions.

This thesis investigates the problem of identifying cracks using an array of strain measurements. It presents analytical methods and computational tools that are required to identify cracks from strain measurements. It also addresses the experimental design problem related to finding the optimal location, orientation, number and density of sensors for reliable detection, along with the computational difficulties involved.

The objective of the present study is twofold. Firstly, a methodology for the estimation of the crack parameters based on a statistical system identification methodology is presented. The crack parameters may include crack location, size and orientation. Their values are estimated using measured data from a structure subjected to static loading. The Bayesian approach to statistical modeling uses probability as a way of quantifying the plausibilities associated with the various models and the values of the parameters of these models given the observed data [14-19]. Probability distributions are used to quantify the various uncertainties in the values of the crack parameters and these distributions are then updated based on information contained in the measured data. The location and size of damage is inferred from the most probable values of the crack

parameters obtained as the ones that maximize the posterior probability distribution of the parameters, given the measured data.

Secondly, a formulation for the optimal design of sensor configuration for crack identification is presented based on the information entropy measure. Previous work addressing the issue of optimally locating a given number of sensors in a structure has been carried out by several investigators. In particular, information theory based approaches (e.g. [20-23]) have been developed to provide rational solutions to several issues encountered in the problem of selecting the optimal sensor configuration. These approaches are closely correlated with the problem of identification and damage detection using vibrational or modal properties. Herein, the information entropy is used to measure the quality of information that can be extracted from the data used to detect a crack. The optimal strain sensor configuration (position and orientation of strain sensors) is obtained as the one that minimizes the information entropy. An important advantage of the information entropy measure is that it allows us to make comparisons between sensor configurations involving a different number of sensors in each configuration [23-25]. The information entropy is particularly useful for trading-off cost of instrumentation with information gained from additional sensors about the condition of the structure, thus making cost-effective decisions regarding optimal instrumentation.

The presentation in this work is organized as follows. In Chapter 2 the crack parameter identification methodology is presented for the general case of a cracked structure and strain measurements. In Chapter 3 a formulation for the design of the optimal sensor configuration for crack identification based on the information entropy measure is presented. Both the crack estimation problem and the optimal sensor

configuration problem are formulated as highly non-convex optimization problems. Chapter 4 briefly reviews a hybrid optimization algorithm combining evolutionary and gradient-based algorithms for the estimation of the global optima in both problems of crack identification and optimal sensor location. In Chapter 5 the effectiveness of the proposed identification methodology and computational algorithms is illustrated for the case of crack in a thin plate subjected to uniform biaxial tension. The simulated data are generated by a computational mechanics problem simulating the behavior of a bounded plate with crack, adding noise in the predictions in order to simulate the effect of measurement error. In order to simulate modeling error the model used to predict the strain field is based on analytical solutions for the strain field available for the case of infinite plate dimensions. In addition, optimal sensor configurations using the proposed computational algorithms are derived and their effectiveness in improving crack detectability is explored. Finally, the conclusions are summarized in Chapter 6.

CHAPTER 2

BAYESIAN FORMULATION FOR IDENTIFYING CRACK PARAMETERS (LOCATION, SIZE AND ORIENTATION)

Consider one or more cracks on a structure subjected to far field static loading (e.g. distributed stress, force, etc.). The objective is to identify the crack locations, sizes and orientations using measured data such as strain measurements. For this, a vector of parameters $\underline{\theta} \in R^{N_\theta}$ defining the crack locations, sizes, and orientations is introduced and the problem of crack identification is equivalent to the problem of estimating the value of the parameter set $\underline{\theta}$.

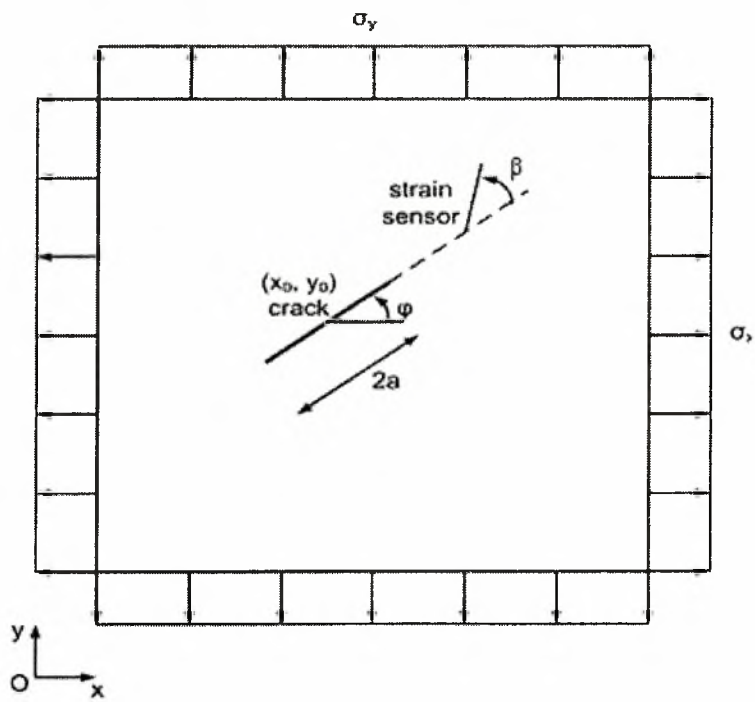

Figure 1. Case of a crack of length 2a in a plate subjected to biaxial tension

Specifically, consider the case of a single crack of length $2a$ in a bounded plate, shown in Figure 1, subjected to biaxial tension. This plate could model a part of a larger structure as in Figure 2. Let the crack have an orientation of angle ϕ and its center be located at (x_0, y_0) with respect to a coordinate system. A parameter vector $\underline{\theta}$ that completely defines the crack and is to be identified, involves crack location (x_0, y_0), length $2a$ and orientation ϕ so as $\underline{\theta} = \{x_0, y_0, a, \phi\}$. In the case of unknown loading, far field stresses σ_x, σ_y should be included in $\underline{\theta}$ so that the parameter set $\underline{\theta} = \{x_0, y_0, a, \phi, \sigma_x, \sigma_y\}$.

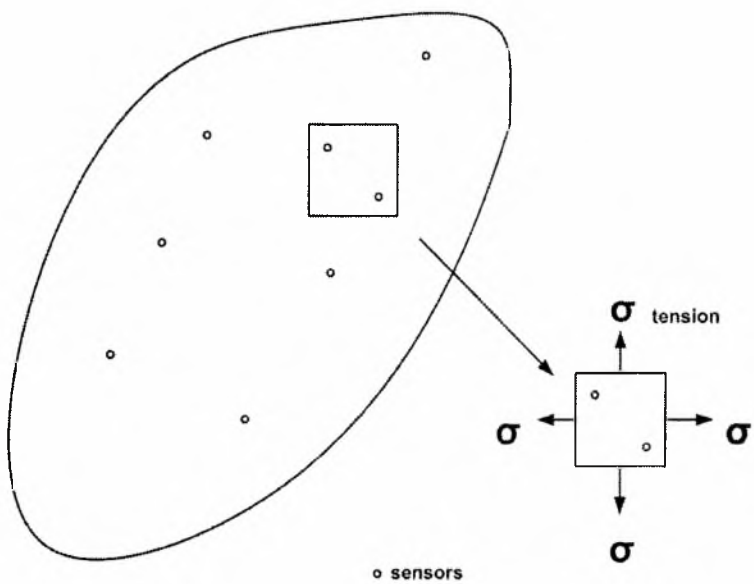

Figure 2. Plate as a part of a larger structure

A Bayesian statistical system identification methodology is used to estimate the values of the parameter set $\underline{\theta}$ and their associated uncertainties using the information provided from test data as follows. Let $D = \{y^{(m)}(\underline{r}_i, \beta_i),\ i = 1,\ldots,N_0, m = 1,\ldots,N\}$ be the measured data, where $\underline{r}_i$ is the position vector indicating the location of the *i*-th measurement, β_i is the angle indicating the direction of the *i*-th measurement, N_0 is the number of sensors in a sensor array and N is the number of data sets available from measurements at different time instants. Let M be a class of models parameterized by the parameter set $\underline{\theta}$, simulating the behavior of the structure with cracks. Let also $q^{(m)}(\underline{r};\beta;\underline{\theta})$ be the response prediction at location $\underline{r}$ and direction β from a model in the class M corresponding to a particular value of the parameter set $\underline{\theta}$. Herein, the model class is associated with the solution of the stress and strain field model around a crack tip. These solutions can be provided by analytical expressions available for infinite plates or can be given from computational finite element models for bounded plates. Thus, each model class corresponds to different modeling assumptions that can affect the reliability of the methodology for detecting cracks.

The measured response and the model response predictions satisfy the prediction error equation

$$y^{(m)}(\underline{r}_i, \beta_i) = q^{(m)}(\underline{r}_i, \beta_i; \underline{\theta}) + n^{(m)}(\underline{r}_i, \beta_i; \underline{\theta}) \qquad i = 1,\ldots,N_0 \quad , m = 1,\ldots,N \qquad (1)$$

where $n^{(m)}(\underline{r}_i, \beta_i; \underline{\theta})$ is model prediction error that is due to modeling error and measurement noise. The prediction error in the $\underline{r}_i$ location with orientation β_i is

assumed to be a zero-mean Gaussian variable, $n^{(m)}(\underline{r}_i, \beta_i; \underline{\theta}) \sim N(0, s_i^2)$, with variance s_i^2.

According to the Bayesian system identification methodology [15], the values of crack parameters $\underline{\theta}$ and the prediction error parameters $\underline{s} = (s_1, s_2, ..., s_N)$ are modeled by probability density functions (PDF) that quantify the plausibility of each possible value of the crack parameter set $\underline{\theta}$ and prediction error parameter set $\underline{s}$. Applying the Bayes' theorem and assuming independence of the prediction errors, the updating posterior PDF $p(\underline{\theta}, \underline{s} | D)$ of the set of parameters $(\underline{\theta}, \underline{s})$ given the measured data D takes the form [19]:

$$p(\underline{\theta}, \underline{s} \mid D) = \frac{c_1}{\left(\sqrt{2\pi}\right)^{N_0 N} \rho(\underline{s})} \exp\left[-\frac{N_0 N}{2} J(\underline{\theta}; \underline{s})\right] \pi(\underline{\theta}, \underline{s}) \tag{2}$$

where $J(\underline{\theta}, \underline{s}) = \frac{1}{N_0} \sum_{i=1}^{N_0} \frac{1}{s_i^2} J_i(\underline{\theta})$, is the overall weighted measure of fit between measured and model predicted responses for all measurement locations,

$$J_i(\theta) = \frac{1}{N} \sum_{m=1}^{N} \left(y^{(m)}(\underline{r}_i, \beta_i) - q^{(m)}(\underline{r}_i, \beta_i; \underline{\theta})\right)^2 \tag{3}$$

is the measure of fit between measured and model predicted response at the *i* measured location, $\rho(\underline{s}) = \prod_{j=1}^{N_0} s_j^N$ is a scalar function of the prediction error parameter set $\underline{s}$, $\pi(\underline{\theta}, \underline{s})$ is the prior distribution for the parameter sets $\underline{\theta}$ and $\underline{s}$ and c_1 is a normalizing constant chosen such that the PDF in (2) integrates to one. Assuming that $\underline{\theta}$ and $\underline{s}$ are independent prior to the collection of data, the prior distribution $\pi(\underline{\theta}, \underline{s})$ takes the form $\pi(\underline{\theta}, \underline{s}) = \pi_\theta(\underline{\theta}) \pi_s(\underline{s})$, where $\pi_\theta(\underline{\theta})$ and $\pi_s(\underline{s})$ are the prior distribution for the parameter sets $\underline{\theta}$ and $\underline{s}$, respectively.

Using the total probability theorem, the marginal probability distribution $p(\underline{\theta} \mid D)$ for the structural model parameters $\underline{\theta}$ is given by $p(\underline{\theta} \mid D) = \int p(\underline{\theta}, \underline{s} \mid D)\, d\underline{s}$. For a non-informative (uniform) prior distribution $\pi_s(\underline{s})$ the integration with respect to $\underline{s}$ can be carried out analytically to yield [16,18]

$$p(\underline{\theta} \mid D) = c_2 \prod_{i=1}^{N_0} \left[J_i(\underline{\theta}) \right]^{-0.5(N-1)} \pi_\theta(\underline{\theta}) \tag{4}$$

where c_2 is a normalizing constant ensuring that the PDF in (4) integrates to one. The updated PDF $p(\underline{\theta} \mid D)$ describes completely the uncertainty in the parameter set $\underline{\theta}$ given the data. In the next section, the updated PDF will be used for designing the optimal sensor configuration.

The optimal value $\hat{\underline{\theta}}_{opt}$ of the parameter set $\underline{\theta}$ is obtained by maximizing $p(\underline{\theta} \mid D)$ in (4). Equivalently, using (4), and assuming a uniform prior distribution for $\underline{\theta}$, the optimal values $\hat{\underline{\theta}}_{opt}$ is given by

$$\hat{\underline{\theta}}_{opt} = \arg\min_{N_0} \sum_{i=1}^{N_0} \ln J_i(\underline{\theta}) \tag{5}$$

In the special case for which $s_1 = s_2 = \ldots = s_{N_0}$, i.e. the values of the prediction error parameters are assumed to be the same, independently of the measured location, the updated PDF $p(\underline{\theta} \mid D)$ of the model parameters $\underline{\theta}$ takes the form

$$p(\underline{\theta} \mid D) = c_3 [J(\underline{\theta}; \underline{1})]^{-(N_0 N - 1)/2} \tag{6}$$

while the optimal value $\hat{\underline{\theta}}_{opt}$ of the parameter set $\underline{\theta}$ is given by

$$\hat{\underline{\theta}}_{opt} = \arg\min_{N_0} \sum_{i=1}^{N_0} J_i(\underline{\theta}) \tag{7}$$

The optimal value $\hat{\underline{\theta}}_{opt} = \{x_{0opt}, y_{0opt}, a_{opt}, \phi_{opt}\}$ of the parameter set $\underline{\theta} = \{x_0, y_0, a, \phi\}$ specifies the most probable location (x_{0opt}, y_{0opt}) of the crack, the most probable half crack length a_{opt}, and the most probable orientation ϕ_{opt} of the crack. The uncertainties in these values is completely defined by the probability distribution $p(\underline{\theta} \mid D)$ given in (4) or (6).

CHAPTER 3

OPTIMAL SENSOR CONFIGURATION METHODOLOGY

3.1 Information Entropy

The updated PDF $p(\underline{\theta} \mid D)$ in (4) specifies the plausibility of each possible value of the crack parameters. It provides a spread of the uncertainty in the parameter values based on the information contained in the measured data. A unique scalar measure of the uncertainty in the estimate of the crack parameters $\underline{\theta}$ is provided by the information entropy, defined by [23]:

$$H(\underline{\delta}, D) = E_{\theta}\left[-\ln p(\underline{\theta}|D)\right] = -\int \ln p(\underline{\theta}|D)\, p(\underline{\theta}|D) d\theta \tag{8}$$

where E_{θ} denotes mathematical expectation with respect to $\underline{\theta}$, and $\underline{\delta} \in R^{3N_0}$ is the sensor configuration vector, with elements the sensors' coordinates and orientations. The information entropy depends on the available data $D \equiv D(\underline{\delta})$ and the sensor configuration vector $\underline{\delta}$.

An asymptotic approximation of the information entropy, valid for large number of data ($NN_0 \to \infty$), is available [24] which is useful in the experimental stage of designing an optimal sensor configuration. The asymptotic approximation is obtained by substituting (4) into (8) and observing that the resulting integral can be re-written as Laplace-type integrals which can be approximated by applying Laplace method of asymptotic expansion [26]. Specifically, it can be shown that for a large number of measured data, *i.e.* $N_0 N \to \infty$, the following asymptotic results hold for the information entropy [25]

$$H(\underline{\delta}, D) \sim H(\underline{\delta}; \hat{\underline{\theta}}, \hat{\underline{s}}) = \frac{1}{2} N_\theta \ln(2\pi) - \frac{1}{2} \ln[\det h(\underline{\delta}; \hat{\underline{\theta}}, \hat{\underline{s}})] \tag{9}$$

where $\hat{\underline{\theta}} \equiv \hat{\underline{\theta}}(\underline{\delta}, D) = \arg\min_{\theta} J(\underline{\theta}; D)$ is the optimal value of the parameter set $\underline{\theta}$ that minimizes the measure of fit $J(\underline{\theta}; D)$ given in (3), $h(\underline{\delta}; \hat{\underline{\theta}}, \hat{\underline{s}})$ is an $N_\theta \times N_\theta$ positive definite matrix defined and asymptotically approximated by [25]

$$h(\underline{\delta}; \hat{\underline{\theta}}, \hat{\underline{s}}) = -\nabla_{\underline{\theta}} \nabla_{\underline{\theta}}^T \ln[J(\underline{\theta}; D)]^{-N_0 N}\Big|_{\underline{\theta}=\hat{\underline{\theta}}} \sim Q(\underline{\delta}, \hat{\underline{\theta}}, \hat{\underline{s}}) \qquad as \quad N_0 N \to \infty \tag{10}$$

in which $\nabla_{\underline{\theta}} = \left[\frac{\partial}{\partial \theta_1} \cdots \frac{\partial}{\partial \theta_{N_\theta}} \right]^T$ is the usual gradient vector with respect to the parameter set $\underline{\theta}$, and $\hat{\underline{s}}$ is the optimal prediction error variance. The matrix $Q(\underline{\delta}; \underline{\theta}, \underline{s})$ appearing in (10) is a positive semi-definite matrix of the form

$$Q(\underline{\delta}; \underline{\theta}, \underline{s}) = \sum_{j=1}^{N_0} \frac{\delta_j}{\hat{s}_j^2} P^{(j)}(\underline{\theta}) \tag{11}$$

known as the Fisher information matrix [21] and containing the information about the values of the crack parameters $\underline{\theta}$ based on the data from all measured positions specified in $\underline{\delta}$, while the optimal prediction error variances $\hat{s}_j^2$ are given by $\hat{s}_j^2 = J_j(\hat{\underline{\theta}})$. The matrix $P^{(j)}(\underline{\theta})$ in (11) is a positive semi-definite matrix given by

$$P^{(j)}(\underline{\theta}) = \frac{1}{N} \sum_{m=1}^{N} \nabla_{\underline{\theta}} q^{(m)}(\underline{r}_j, \beta_j; \underline{\theta}) \, \nabla_{\underline{\theta}}^T q^{(m)}(\underline{r}_j, \beta_j; \underline{\theta}) \tag{12}$$

containing the information about the values of the parameters $\underline{\theta}$ based on the data from one sensor placed at the location $\underline{r}_j$ and having orientation β_j. The matrix $P^{(j)}(\underline{\theta})$ depends only on the response of the optimal model at the measurement location j, while it is independent of the sensor configuration vector $\underline{\delta}$.

It should be noted that the resulting asymptotic value of the information entropy, given in (10), does no longer depend explicitly on the measured response data D. The only dependence of the information entropy on the data comes implicitly through the optimal values $\hat{\underline{\theta}} \equiv \hat{\underline{\theta}}(\underline{\delta}, D)$ and $\hat{s}^2 = J(\hat{\underline{\theta}}; D)$. Consequently, the information entropy is completely defined by the optimal value $\hat{\underline{\theta}}$ of the model parameters and the optimal prediction error $\hat{\underline{s}}$ expected for a set of test data.

Using the positive semi-definiteness of the matrices $P^{(j)}(\underline{\theta})$ and the structure of $Q(\underline{\delta}; \underline{\theta}, \underline{s})$, it can be readily shown [25] that the value of the information entropy decreases as additional sensors are placed in a structure. Given the interpretation of the information entropy as a measure of the uncertainty in the parameter estimates, this should be intuitively expected since adding one or more sensors in the structure will have the effect of providing more information about the system parameters. Moreover, it can be shown [24] that the minimum (maximum) information entropy value corresponding to the optimal (worst) sensor configuration for L sensors is a decreasing function of the number of sensors L.

3.2 Design of Optimal Sensor Configuration

In damage detection techniques the aim is to design sensor configurations such that the resulting measured data are most informative about the model parameters. Since the information entropy, introduced in (8) as a measure of the uncertainty in the crack parameters, gives the amount of useful information contained in the measured data, the optimal sensor configuration is selected as the one that minimizes the information entropy [23]. That is,

$$\underline{\delta}_{best} = \arg\min_{\underline{\delta}} H(\underline{\delta}; \hat{\underline{\theta}}, \hat{\underline{s}}) \tag{13}$$

However, in the initial stage of designing the experiment, the data are not available and thus an estimate of the optimal crack parameters $\hat{\underline{\theta}}$ and $\hat{\underline{s}}$ cannot be obtained from analysis. In order to proceed with the design of the optimal sensor configuration, this estimate has either to be assumed or its uncertainty has to be accounted for. In practice, the optimal sensor configuration designs are based on user-selected nominal values of the optimal model parameters $\hat{\underline{\theta}}$ and $\hat{\underline{s}}$ that are representative of the structure under study. It is worth pointing out that, as a result of the asymptotic approximation of the information entropy, the selection of the optimal sensor configuration is based solely on a nominal model, ignoring details from the measured data that are unavailable in the initial stage of experimental design.

3.3 Prediction Error Variance Model

An analysis of the prediction error variance $s_i^2, i = 1,..., N_0$ is next presented. For the prediction error, it holds that

$$n^{(m)}(\underline{r}_i, \beta_i; \underline{\theta}) = n_{model}(\underline{r}_i, \beta_i; \underline{\theta}) + n_{meas}^{(m)}(\underline{r}_i, \beta_i; \underline{\theta}) \qquad i = 1,..., N_0, m = 1,..., N \tag{14}$$

where $n_{model}(\underline{r}_i, \beta_i; \underline{\theta})$ accounts for the model error and $n_{meas}^{(m)}(\underline{r}_i, \beta_i; \underline{\theta})$ accounts for the measurement error. Assuming independence between the measurement error and model error, the variance s_i^2 of the total prediction error is given in the form

$$s_i^2 = s_{i,\text{meas}}^2 + s_{i,\text{model}}^2 \tag{15}$$

where $s^2_{i,\text{meas}}$ is the variance of the measurement error and $s^2_{i,\text{model}}$ is the variance of the model error. In order to proceed with the optimal sensor configuration design, the designer has to assume values for the individual variances in (15). Such assumptions may depend on the nature of the problem analyzed. Most studies on optimal sensor location assume that the variance of the measurement and model errors are constant, independent of the response. However, in the crack problems considered in this study, it may be reasonable to assume that the variance of the model error is proportional to the response. In addition, the response may be extremely sensitive to very small variations of the measurement location as in the case of measuring strains close to the crack tip. Specifically, due to $1/\sqrt{r}$ variation of the strain distribution, where r is the distance from the crack tip, small variations in the sensor location, due to inaccurate sensor location, may result in extremely high variations in the response close to the crack tip. Thus, the sensitivity of the measured response to sensor location may play an important role in defining the measurement and model error. To properly account for these variations, it is reasonable to assume that the error is a function of the sensitivity of the response to variations in the sensor positions. Usually this error and the corresponding prediction error variance may be considered to be a function of the measured response or its spatial derivatives.

Adding all these errors together, one can derive the following expression for the variance of the prediction error

$$s_i^2 = c_0^2 + c_{r_i}^2 q^2(\underline{r}_i, \beta_i; \underline{\theta}) + c^2(q) \tag{16}$$

where the first term accounts for constant errors, independent of the response, the second term accounts for prediction errors that depend on the strength of the response predicted

by the model, and the third term accounts for prediction errors that depend on the details of the response q. Further analysis and estimation of this variance for the specific case of a single crack in a thin plate is presented in Chapter 5.

CHAPTER 4

OPTIMIZATION – COMPUTATIONAL ISSUES

4.1 Hybrid Optimization Algorithm

Both optimization problems (5) or (7) and (13), related to the estimation of the crack parameters and the estimation of optimal sensor configuration, result in multiple global/local optima. Conventional gradient-based local optimization methods are unable to handle efficiently multiple local optima and may present difficulties in estimating the global minimum. They lack reliability in dealing with the optimization problem since convergence to the global minimum is not guaranteed. Evolutionary algorithms [27] are more appropriate and effective to use in such cases. Evolutionary algorithms are random search algorithms that explore better the parameter space for detecting the neighborhood of the global optimum. They are based on a randomly initialized population of search points in the parameter space, which by means of selection, mutation, and recombination evolves towards better and better regions in the search space. Details on theoretical developments of evolution strategies (ES) can be found in Beyer [28]. A disadvantage of ES is their slow convergence in the neighborehood of the global optimum since they do not exploit the gradient information. For this, a hybrid optimization algorithm is used that exploits the advantages of evolutionary and gradient-based methods. Specifically, an evolution strategy is first used to explore the parameter space and detect the neighborhood of global minimum. Then the method switches to a gradient-based algorithm starting with the best estimate obtained from the evolutionary algorithm and using gradient information to accelerate converge to the global optimum. Due to the

random nature of the initial population used in ES, the proposed hybrid optimization algorithm is effective of determining multiple global minima by running the algorithm several times and storing the optimal solution of each run into an optimal set of solutions. Depending on the initial population in each run, the algorithm may converge to a different global optimum in the parameter space. As the number of runs increases, the optimal set of solutions usually contains all optima solutions for the problem.

4.2 Heuristic Algorithm for Optimal Sensor Configuration

A more systematic and computationally very efficient approach for obtaining a good sensor configuration for a fixed number of N_0 sensors is to use a sequential sensor placement algorithm as follows. The positions of N_0 sensors are computed sequentially by placing one sensor at a time in the plate, starting with a minimum number of $N_{\min}$ sensors, at a position and orientation that results in the highest reduction in information entropy. The minimum number of sensors $N_{\min}$ used is the one that corresponds to an identifiable crack parameter set. This is investigated through the determinant of the matrix Q in (12), since when $\det(Q) \to 0$ then the number of sensors used is not enough to create an array of sensors whose measurements will result in an identifiable model. So the positions of the first $N_{\min}$ sensors are chosen as those that give the highest reduction in the information entropy for $N_{\min}$ sensors. Given the optimal positions of the first $N_{\min}$ sensors, the position of the next sensor is chosen as the one that gives the highest reduction in the information entropy computed for $(N_{\min}+1)$ sensors with the positions of the first $N_{\min}$ sensors fixed at the optimal ones already computed in the first step.

Continuing in a similar fashion, given the positions of $i-1$ $\left(i \geq N_{\min} + 1 \right)$ sensors in the structure computed in the previous $i-1$ steps, the position of the next ith sensor is obtained as the one that gives the highest reduction in the information entropy for i sensors with the positions of the first $i-1$ sensors fixed at the optimal ones already obtained in the previous $i-1$ steps. This procedure is continued for up to N_0 sensors. This algorithm is referred to as the sequential sensor placement algorithm and has been first introduced in [25] to handle the discrete optimization problem. The sequential sensor placement algorithm, when applied to discrete-variable optimization problems, was shown to give sensor configurations with corresponding information entropies that are extremely close to the minimum information entropy. Its effectiveness to continuous-variable optimization problem arising in the present study will be investigated in the application section.

CHAPTER 5

APPLICATIONS

The effectiveness of the proposed methodology is demonstrated using simulated strain measurements $\hat{\varepsilon}$ for the mode I crack problem of Figure 3 representing a bounded plate with dimensions L_1 and L_2, under uniform biaxial tension ($\sigma_x = \sigma_y = \sigma$). Since there are no experimental data available, simulated measured data are generated from a finite element model of the corresponding problem created with COMSOL Multiphysics [29] for the various crack configuration assumed and for specimen size $L_1 = L_2 = ea$. Details for generating the strain field using finite element modeling are given in Appendix B. Zero-mean Gaussian white noise errors are added to the finite element model results in order to simulate the effect of measurement error. So the "measured data" $\hat{\varepsilon}$ are generated as follows:

$$\hat{\varepsilon} = \varepsilon_{FEM}\left(1+\eta\right) \tag{17}$$

where ε_{FEM} are the strain values obtained from the finite element model for a given value of e, and η is a Gaussian variable with zero mean and standard deviation s.

Model predictions of the strain field $\varepsilon(x, y)$ near and far from the crack tip are provided for various crack configurations by an analytical solution [30] available for this stress state, provided that the dimensions L_1 and L_2 of the plate are infinite, or for practical applications much larger than the crack length, i.e. $e \gg 10$.

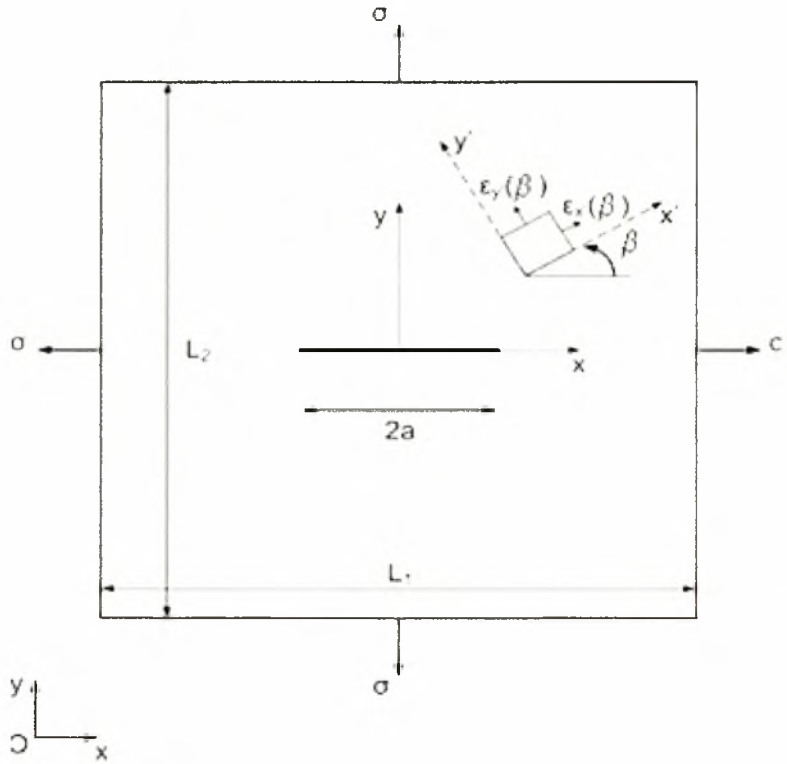

Figure 3. Case of a crack of length 2a in a bounded plate subjected to uniform biaxial tension at far field

Specifically, the stresses for an infinite plate can be determined as

$$\sigma_x = \mathrm{Re}\, Z - y\, \mathrm{Im}\, Z'$$

$$\sigma_y = \mathrm{Re}\, Z + y\, \mathrm{Im}\, Z' \tag{18}$$

where the stress function Z is given by

$$Z = \frac{\sigma z}{\sqrt{z^2 - a^2}}, \tag{19}$$

where $z = x + iy$ and

$$Z' = \frac{dZ}{dz} \tag{20}$$

Consequently, for plane stress problem the strains are given by

$$\varepsilon_x = \frac{1-\nu}{E}\mathrm{Re}\,Z - \frac{1+\nu}{E} y\,\mathrm{Im}\,Z'$$

$$\varepsilon_y = \frac{1-\nu}{E}\mathrm{Re}\,Z + \frac{1+\nu}{E} y\,\mathrm{Im}\,Z' \tag{21}$$

where E is Young's modulus and ν is Poisson's ratio. Finally, model predictions of normal strains at an element oriented along a particular direction β (see Fig. 3) on the plate can be readily obtained using the well-known transformation formulas

$$\begin{aligned}\varepsilon_{x'}(\beta) &= \frac{\varepsilon_x+\varepsilon_y}{2} + \frac{\varepsilon_x-\varepsilon_y}{2}\cos 2\beta + \frac{1}{2}\gamma_{xy}\sin 2\beta \\ \varepsilon_{y'}(\beta) &= \frac{\varepsilon_x+\varepsilon_y}{2} - \frac{\varepsilon_x-\varepsilon_y}{2}\cos 2\beta - \frac{1}{2}\gamma_{xy}\sin 2\beta\end{aligned} \tag{22}$$

The two different models, the computational model used for simulating measured strain data from a bounded square plate with dimension ea, and the analytical model used for predicting the strain field of an infinite plate structure, are purposely chosen to introduce modeling error always present in structural modeling. One of the purpose of the analysis is to investigate the effect of modeling error on the effectiveness of identification methodology. The size of modeling error depends on the value of the variable e. The smaller the value of e, the less accurate the analytical solution is for describing the strain field in a bounded plate, the higher the size of modeling error is.

In the results presented in this thesis, the material properties are Young's modulus $E = 70\text{GPa}$ and Poisson ratio $\nu = 0.33$. In all cases examined the simulated data were generated for these values of material properties and the following values of crack parameters: position of crack $x_0 = 0.06$, $y_0 = 0.06$, half crack length $a = 0.005$ and crack orientation $\phi = 0$. The modeled plate was subjected to uniform far field stress $\sigma = 100\text{MPa}$.

5.1 Existence of multiple local/global optima

In order to demonstrate the existence of multiple local optima, and therefore the necessity of an efficient global optimization algorithm, we consider the case of small model error ($e = 100$), no measurement error ($\eta = 0\%$) and known far field stresses so as the parameters to be identified in this case are cracks location (x_0, y_0), size (half crack length) a and orientation ϕ. Figure 4 shows the contour plots of the measure of fit in (3), for the sensor configuration shown in Figure 5, as a function of the crack position x_0, y_0 holding the values of the other parameters a and ϕ constant. It is observed from these figures that a highly nonlinear, non-convex, objective function is obtained which involves multiple local optima. The global optimum is in the area around $x = 0.6$, $y = 0.6$ and corresponds to the crack position in the finite element model that produced the measured data $\hat{\varepsilon}$. A gradient-based optimization method with an initial estimate chosen in one of the neighborhoods of the local optima will fail to converge to the global optimum, leading to a sub-optimal solution corresponding to a local optimum.

Specifically, the proposed hybrid optimization algorithm is shown to be effective in avoiding local optima and locating the global one. Evolutionary algorithms are used in these cases in order to estimate the neighbourhood of the global optimum, and then the algorithm is switched to a gradient-based optimization algorithm that can converge quickly to the global optimum. However, in order to find the neighbourhood of the global optimum, evolutionary algorithms require a relatively large number of function evaluations and this makes the proposed approach computationally time consuming.

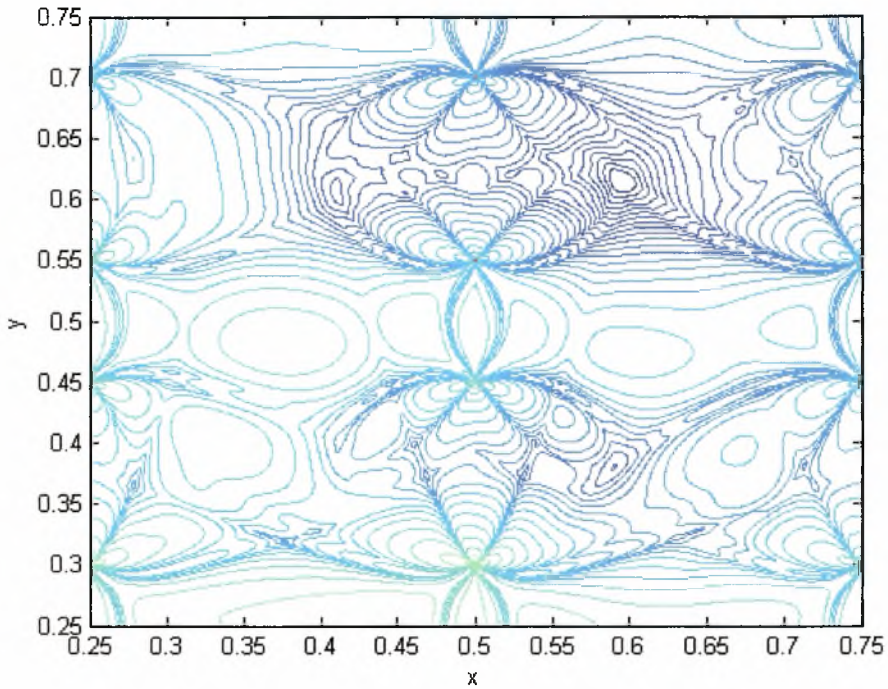

Figure 4: Contour plots of the total mean-square prediction error as a function of the coordinates x, y of the crack center

5.2 Crack Identification Results

At first, results are shown for the same case of small model error ($e=100$), no measurement error ($\eta=0\%$) and crack parameters set $\underline{\theta}=\{x_0, y_0, a, \phi\}$. A grid of 18 sensors was used to measure strains $\varepsilon_x, \varepsilon_y$ in 9 locations as shown schematically in Fig. 5. The optimal values $\underline{\hat{\theta}}_{opt}$ of the cracks parameter set $\underline{\theta}$ are given in Table 1. The far field uniform stress σ is assumed to be given. The crack location, orientation and size predicted by the proposed methodology is also shown in Figure 5 (black line) and is compared to the nominal values of crack location, size and orientation (red line) used to generate the simulated data. It is clear that all parameters for this case were estimated with great accuracy resulting in a complete identification of the location, size and orientation of the crack.

Parameters											
model error e	measurement error η	x_0		y_0		a		ϕ		σ (x100MPa)	
		nominal value (n.v.)	prediction (pr.)	n.v.	pr.	n.v.	pr.	n.v.	pr.	n.v.	pr.
100	0%	0.06	0.0605	0.06	0.0604	0.005	0.00478	0°	0.7°	-	-
100	0%	0.06	0.0608	0.06	0.0603	0.005	0.00535	0°	0.6°	1.0	1.004
100	2%	0.06	0.0606	0.06	0.0597	0.005	0.00517	0°	0.05°	1.0	0.996

Table 1. Identification results for small model error

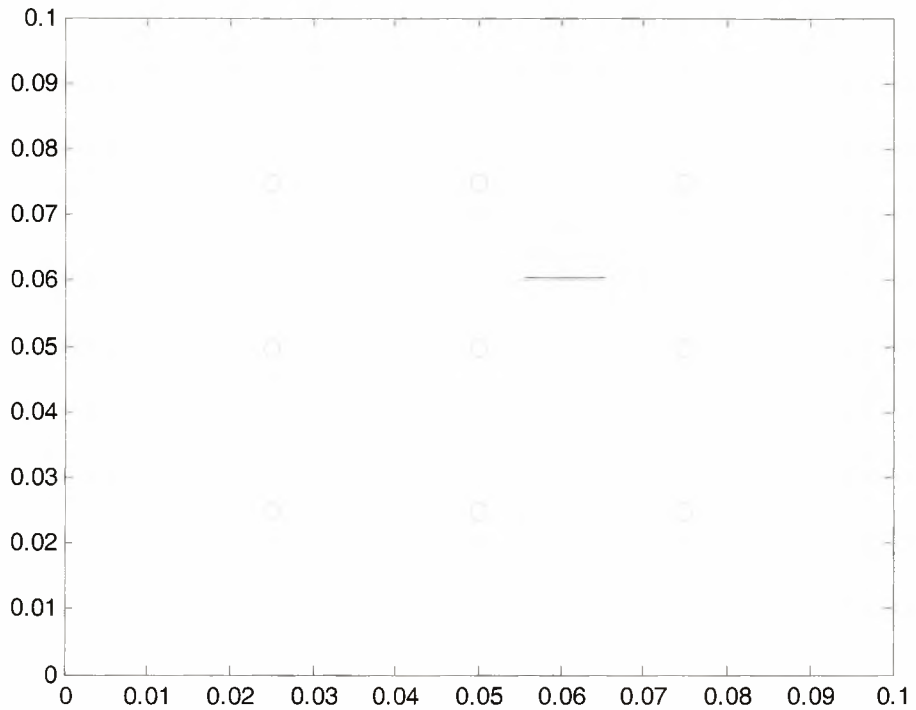

Figure 5: Crack identification using strain measurements $\varepsilon_x, \varepsilon_y$ at 9 locations and considering small model error ($e = 100$) and no measurement error ($\eta = 0\%$)

The problem of estimating the crack parameters set that includes as unknown the far field uniform stress σ is investigated next. The same finite element model is used to produce the simulated data. The 18 sensors array measuring strains $\varepsilon_x, \varepsilon_y$ in 9 locations as shown in Figures 6(a) and (b) is assumed. In the presence of measurement error, simulated data are produced more than once so as to obtain three data sets $N = 3$ comprised of strain measurements $\varepsilon_x, \varepsilon_y$ in the same locations. Figure 6(a) shows results for the case of small modeling error and no measurement error ($e = 100, \eta = 0\%$). Figure 6(b) shows results for same model error but non-zero measurement error of $\eta = 2\%$ in all measured strains. The optimal values of the crack parameters set $\underline{\theta}$ are shown in Table 1.

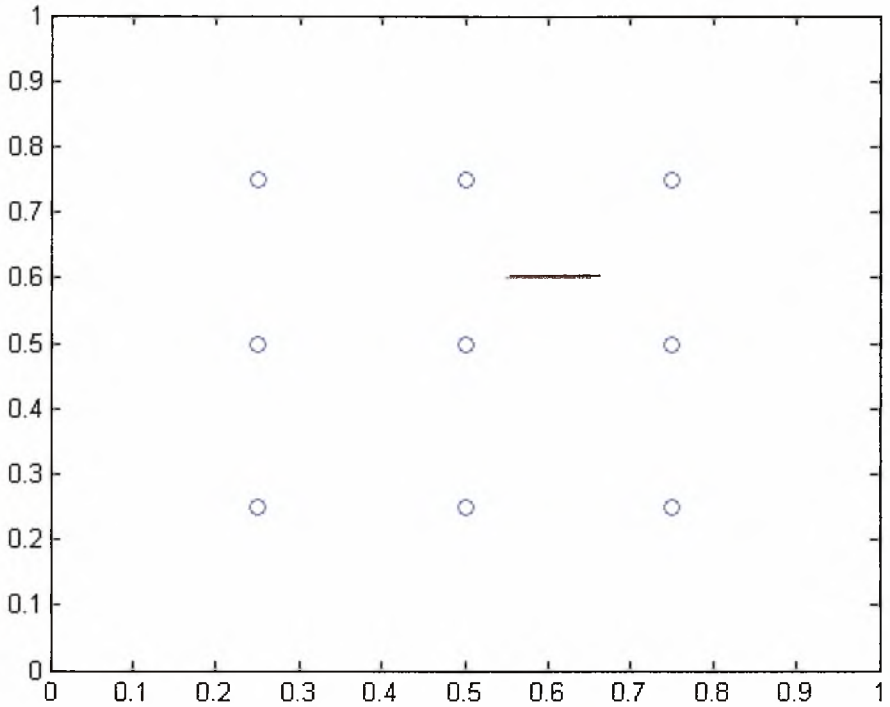

Figure 6a: Crack identification using strain measurements from 18 sensors considering small model error ($e = 100$) and no measurement error ($\eta = 0\%$)

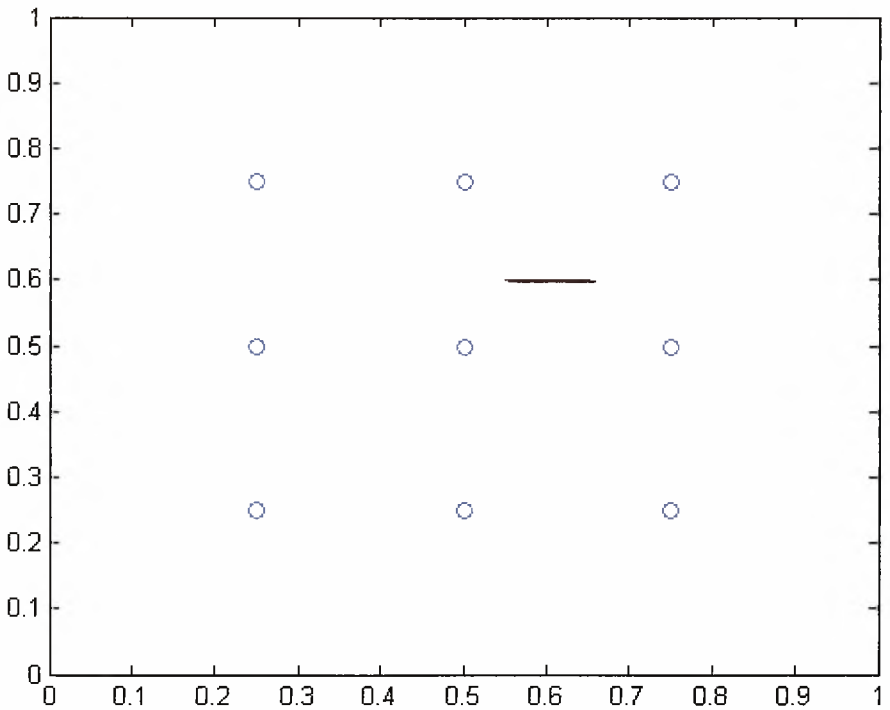

Figure 6b: Crack identification using strain measurements from 18 sensors considering small model error ($e = 100$) and $\eta = 2\%$ measurement error

The additional parameter (far field stress σ) and the presence of 2% noise in measurements do not affect the accuracy of the identified parameters as seen from the results in Table 1 and the predictions of the crack configurations (black lines) in Figures 6(a) and (b).

5.2.1 Sensitivity to Model Error

Next, the effect of model error on the effectiveness of the methodology is investigated. For this, the crack detection problem is considered for the following cases: (a) the case of plate dimensions $L = 100a$ corresponding to small model error $(e = 100)$, (b) the case of plate dimensions $L = 10a$ corresponding to medium model error $(e = 10)$, and (c) the case of plate dimensions $L = 7a$ corresponding to large model error $(e = 7)$. The respective sizes of model error are due to the fact that the analytical solutions used to predict the strain field in the identification method hold only for infinite dimensions and tend to be inaccurate as the ratio $L/a = e$ decreases. An additional $\eta = 2\%$ noise in the measurements is assumed. The crack identification results for the case of $L = 100a$ was already shown in Figure 6b. Results for the cases of $L = 10a$ $(e = 10)$ and $L = 7a$ $(e = 7)$ are shown in Figures 7 and 8 respectively. The optimal values of the parameter set $\underline{\theta}$ are given in Table 2 for the three cases considered. From the results in Table 2 we observe that the increase of the model error from $e = 100$ to $e = 7$ results in a certain loss of accuracy in the identified parameters. Specifically, for medium model error $(e = 10)$ there is a 7% relative error in the estimation of cracks half-length, while in the case of large model error $(e = 7)$ there is a 12% relative error in the estimation of the size of the crack combined with an error of 3% in the estimate of cracks location. Also, the

orientation of the crack predicted by the methodology, is slightely missed by approximately 3° to 4°.

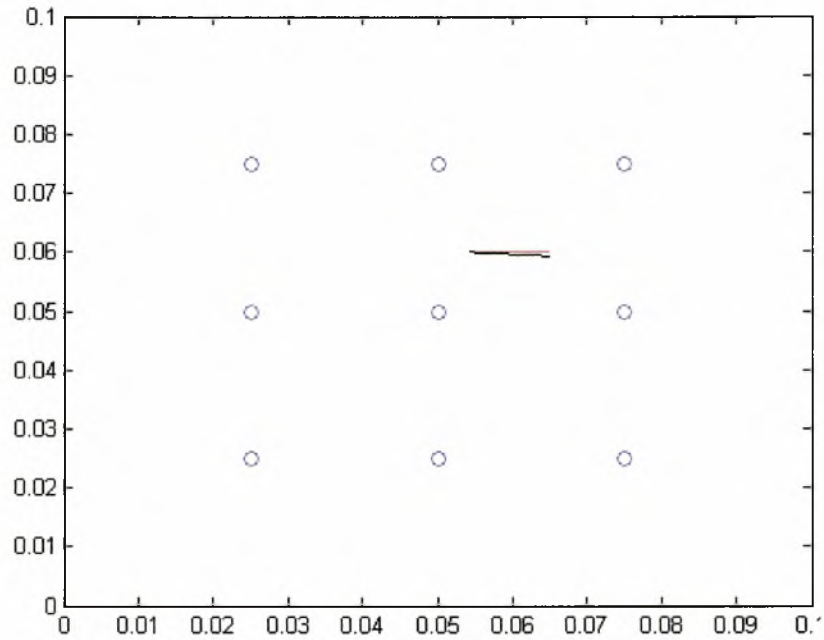

Figure 8: Crack identification using strain measurements from 18 sensors considering medium modeling error and white noise measurement error $n = 2\%$.

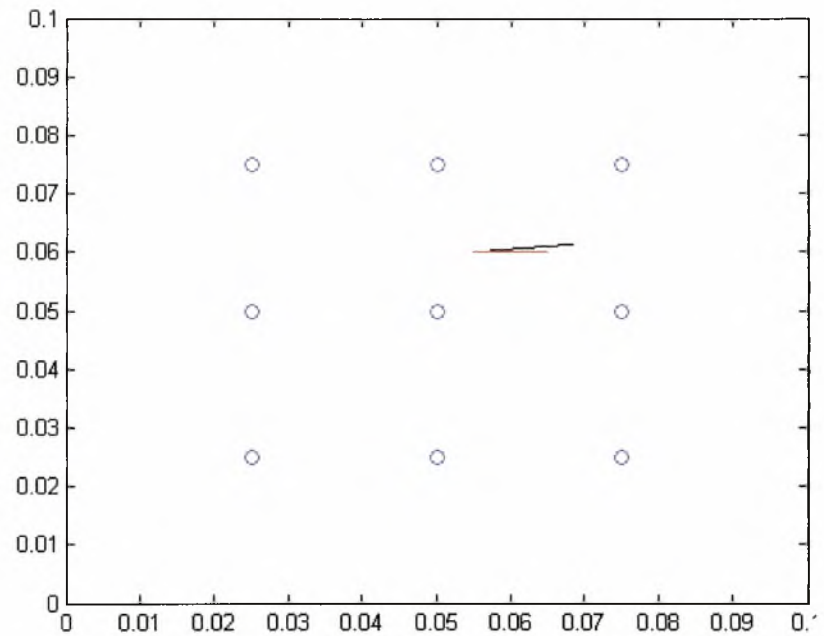

Figure 9: Crack identification using strain measurements from 18 sensors considering large modeling error and white noise measurement error $n = 2\%$.

Parameters											
model error e	measurement error	x_0		y_0		a		ϕ		σ (x100MPa)	
		nominal value (n.v.)	prediction (pr.)	n.v.	pr.	n.v.	pr.	n.v.	pr.	n.v.	pr.
100	2%	0.06	0.0606	0.06	0.0597	0.005	0.00517	0°	0.05°	1.0	0.996
10	2%	0.06	0.05966	0.06	0.05964	0.005	0.00536	0°	3.75°	1.0	0.9885
7	2%	0.06	0.0618	0.06	0.0583	0.005	0.00438	0°	3.1°	1.0	1.0004

Table 2. Identification results for medium (e=10) and large (e=7) model error

5.2.2 Parametric Analysis

Results show that the proposed methodology can efficiently detect a crack in a thin plate, and accurately estimate its size and orientation, as well as the unknown load to which the plate is subjected to. Next, the limits on which this methodology tends to or completely fails to identify the crack are examined. These limits depend on several parameters such as the sensor configuration, the density of the sensors array with respect to the crack size, the measurement direction of the strain sensors, the orientation of the crack etc. The following analysis investigates the effect of these parameters on the accuracy of the identification algorithm.

First, let γ be the distance of the sensor locations in the $3x3$ uniform grid of sensors measuring ε_x, ε_y shown in Figure 10. We introduce the parameter $p_1 = \gamma / a$, where a is the half crack length, and examine the relative errors in the estimation of crack parameters for different values of p_1.

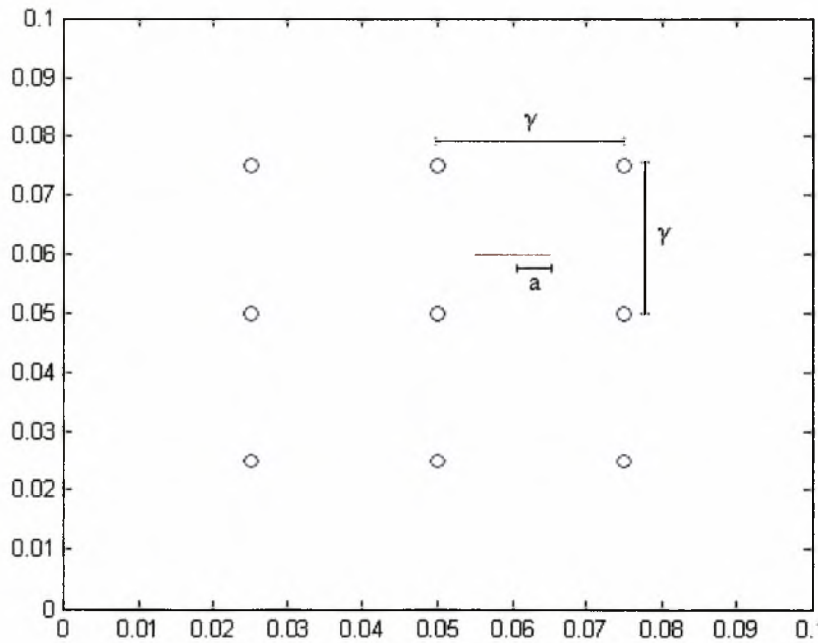

Figure 10: Grid parameter γ and half crack length a

In all results shown next we consider the case of small model error $e = 100$ and measurement error $\eta = 2\%$. The far field uniform stress σ is considered to be unknown. Results for $p_1 = 5$ were already shown in Figure 6b, while for $p_1 < 5$ the methodology identifies accurately all crack parameters. Although this can be understood intuitively, since smaller values of p_1 correspond to denser sensor configuration or equivalently larger crack, it is also confirmed by results.

In Figure 11 the relative error in the estimation of the cracks location and size for larger values of p_1 is presented. It is observed that for $p_1 = 10$ the methodology has failed to detect the crack since the relative error in the coordinates estimation reaches a value of 50% in addition to a 13% relative error in determining the half cracks length.

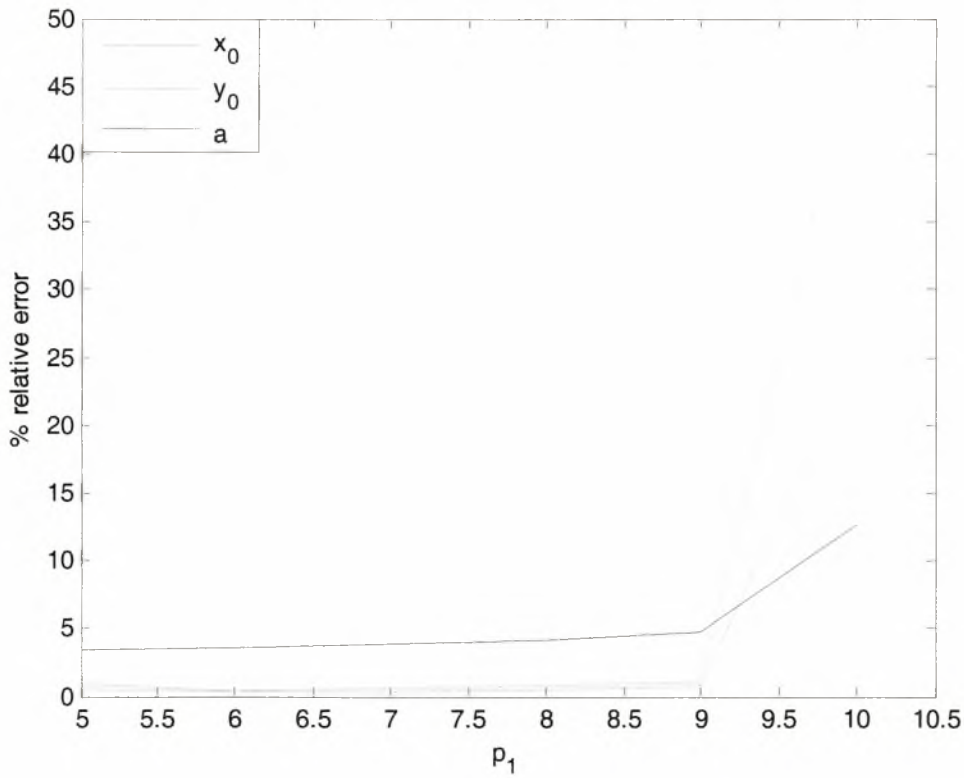

Figure 11: Relative errors in the estimation of x_0, y_0 and a as a function of p_1

For the crack size shown in Figure 10 the value $p_1 = 10$ corresponds to a sensor array with distance γ two times the distance shown in Figure 10. It must be noted here that even in this case, the crack orientation ϕ and the far field stresses σ were accurately estimated.

Of great importance is also the method's dependence on the crack location and especially its distance from the central sensor with respect to the cracks size. For this reason we consider the parameter $p_2 = x_c / \alpha$, where x_c is the distance of the cracks center from the central sensor along the x-axis as shown in Figure 12. Values of the relative errors in the estimated values of cracks location coordinates x_0, y_0 and half crack length a are presented in Figure 13 for value of the ratio $p_1 = \gamma / a = 5$.

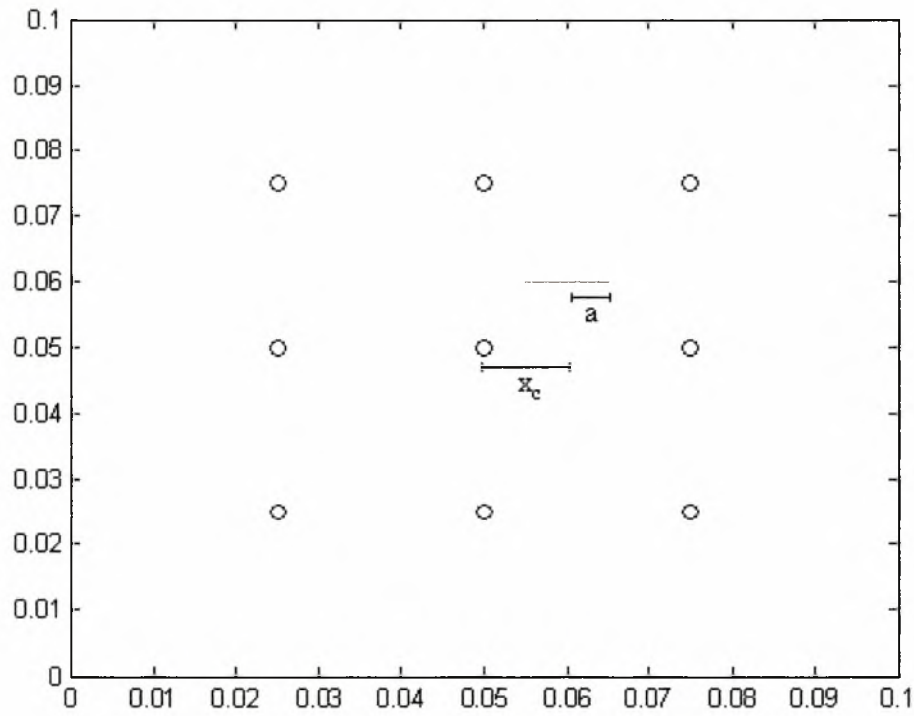

Figure 12: Distance x_c and half crack length a

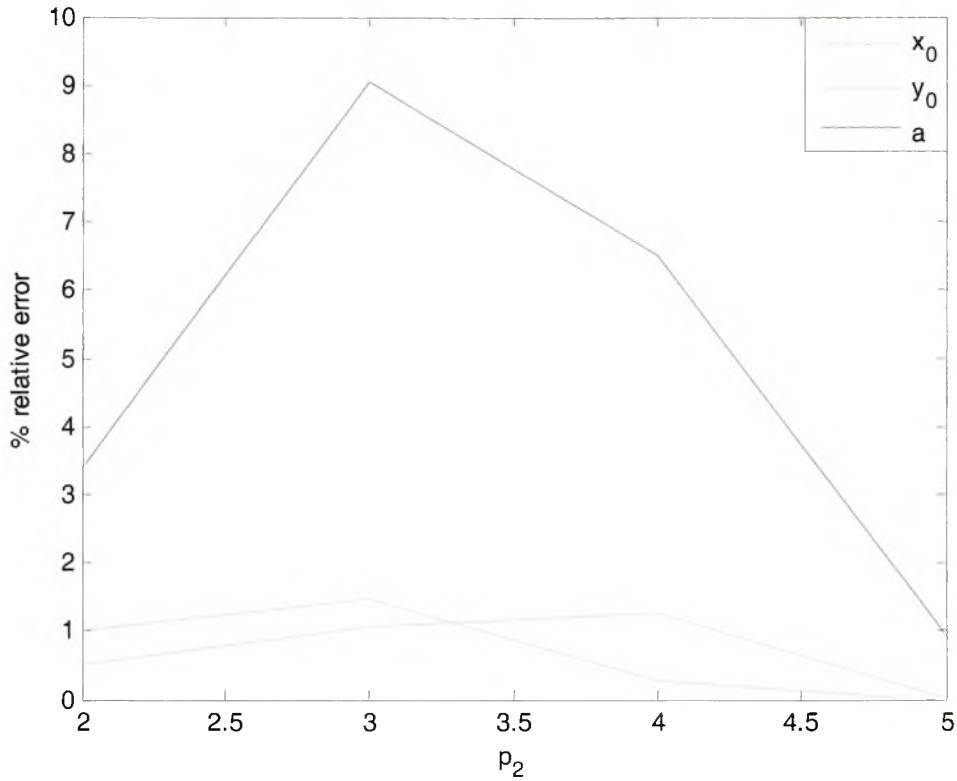

Figure 13: Relative errors in the estimation of x_0, y_0 and a as a function of p_2

It is observed that as the crack moves far from the central sensor, errors in the crack location estimation slightly increase while there is a larger error of about 9% in the estimated half crack length. For $p_2 \geq 4$, the crack approaches another sensor and these errors decrease with the accuracy of the methodology to improve significantly. Despite the errors, it is important that the algorithm identifies the crack parameters in other positions within the grid apart from the one initially considered, as long as the other parameters in the crack problem remain constant.

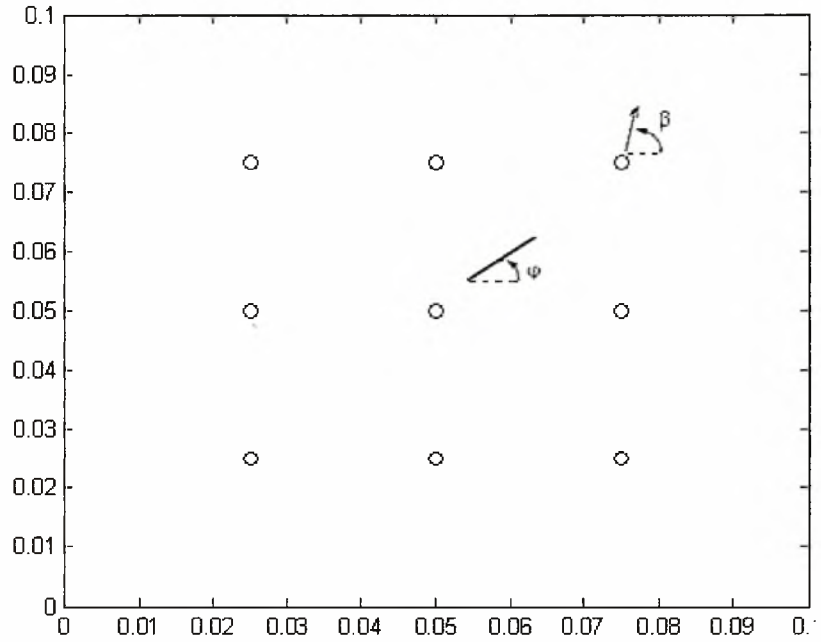

Figure 14: Crack orientation ϕ and measurement direction β

In all results presented before an array of sensors measuring strains in x, y direction was used while the crack had an orientation $\phi = 0°$. This means that strain measurements were obtained simultaneously in parallel and perpendicular directions with respect to the cracks orientation. We examine next the case where 9 instead of 18 sensors are used to measure strains in a direction β, while the crack has an orientation ϕ as shown in Figure 14. The parameter $p_3 = \beta - \phi$ is introduced and for the values $p_3 = 0$ and $p_3 = \pi/2$ identification results are examined as a function of p_1. The value of $p_3 = 0$ corresponds to the case where the strain measurements are parallel to the crack, while the value of $p_3 = \pi/2$ corresponds to strain measurements perpendicular to the crack. A comparison of the relative errors on the estimation of cracks location coordinates x_0, y_0 and half crack length a for the two values of the parameter p_3 are presented in Figure 15, 16 and 17 respectively. It is clear that when measuring strains in a direction parallel to the crack,

the methodology fails to estimate crack parameters for smaller values of the ratio γ/α than the case of strains obtained perpendicular to the crack. This conclusion will be reinforced by the results of the optimal sensor location methodology shown next where for the crack orientation $\phi = 0°$ the methodology results in an optimum measurement direction $\beta = 270°$ for all sensors. We should note here that the use of 9 instead of 18 sensors and one single direction instead of two resulted in a loss of accuracy in the estimation of cracks orientation of approximately $9°$. Moreover, the error in the estimation of half cracks length is large even for small values of $p_1 = \gamma/a$.

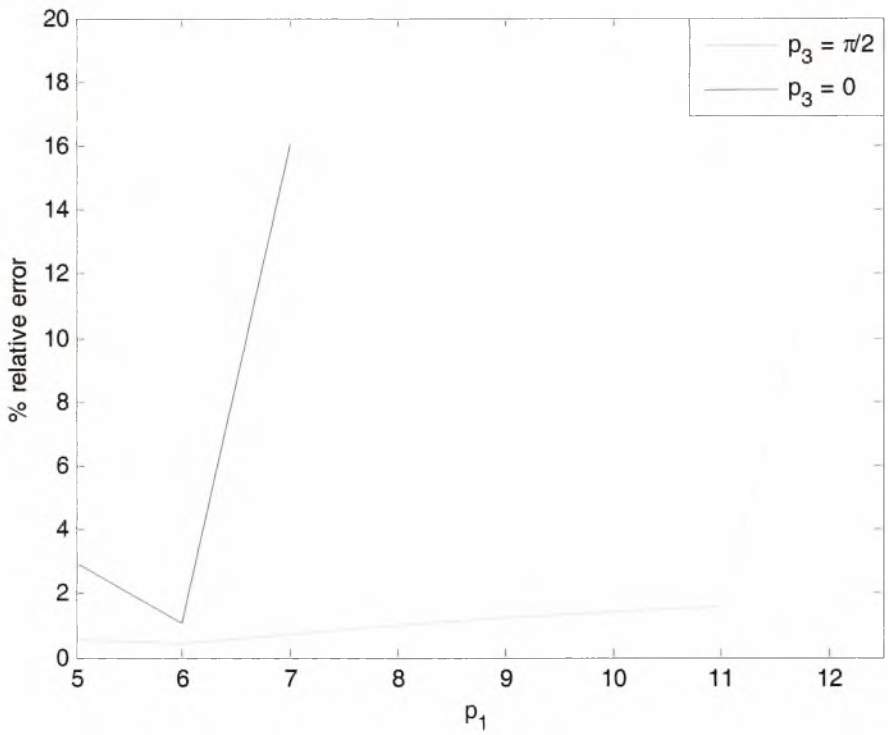

Figure 15: Relative errors in the estimation of x_0 for $p_3 = \pi/2$ and $p_3 = 0$ as a function of p_1

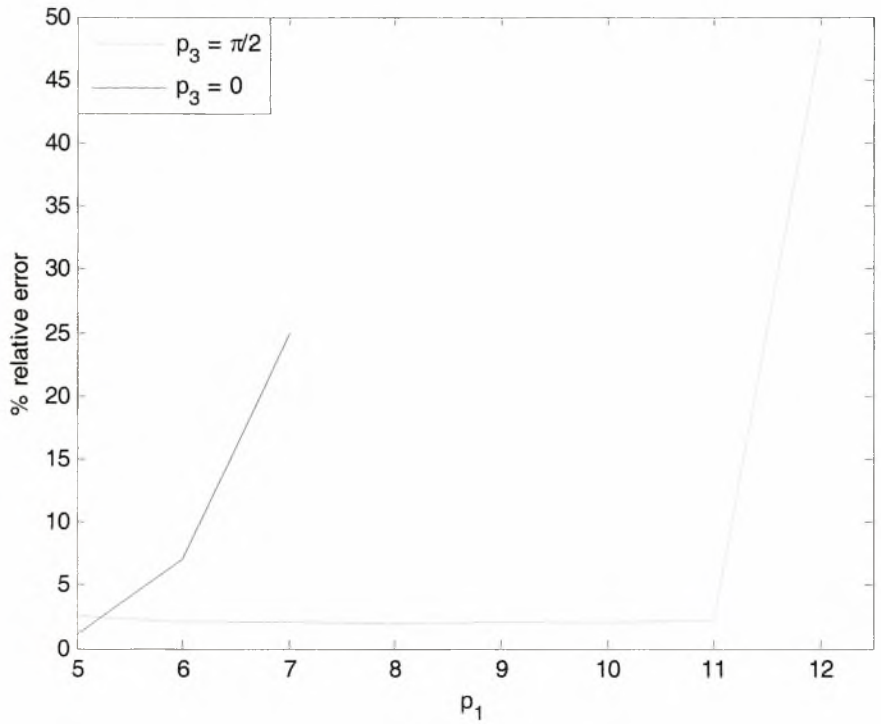

Figure 16: Relative errors in the estimation of y_0 for $p_3 = \pi/2$ and $p_3 = 0$ as a function of p_1

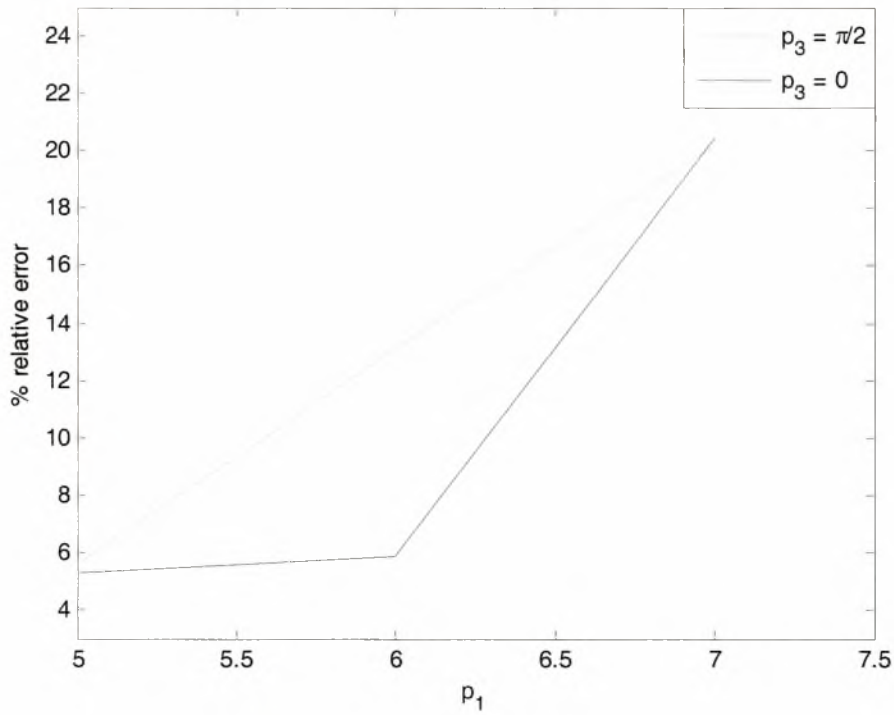

Figure 17: Relative errors in the estimation of a for $p_3 = \pi/2$ and $p_3 = 0$ as a function of p_1

5.3 Optimal Sensor Configurations

Next we estimate the optimal sensor configuration for a given number of sensors using the theoretical analysis presented in Chapter 3. Two cases are considered: in Case A the variables to be estimated are the locations of strain sensors measuring ε_x and ε_y in a measurement location, so the search of the optimal sensor configuration for n sensors corresponds to $n/2$ optimal locations. In Case B in each optimal location corresponds one sensor measuring strain at the direction of β. Thus, the variables to be estimated in the search of the optimal configuration include the location and the direction of measurements as well. In this case the sensor configuration vector $\underline{\delta} \in R^{3N_0}$ includes not only coordinates of each sensor, but angles β of measurement direction as well.

5.3.1 Selection of the Prediction Error

As mentioned in Chapter 3 the estimation of the optimal sensor configuration depends on the selection of the prediction error parameters involved in the prediction error in the prediction error equation (16). In all results presented here, the value of the prediction error variance s^2 is chosen as follows.

First we will define the third term in prediction error equation (16) that depends on the nature of the response. For the strain ε near the crack tip, it holds

$$\varepsilon \sim \frac{a}{\sqrt{r}} = \frac{a(K_I, E, \nu)}{\sqrt{r}} \tag{23}$$

where r is the distance from the crack tip, K_I is the stress intensity factor, E is Young's modulus and ν is Poisson's ratio. Due to the $1/\sqrt{r}$ variation of the strain distribution, small variations in the sensor location may result in extremely high variations in the

response close to the crack tip. To properly account for these extreme variations, it is reasonable to assume that the error is a function of the response's spatial derivatives with respect to r. Considering an inaccurate sensor placement of about Δr, using (23), and selecting the standard deviation of the error to be proportional to the local change $\Delta\varepsilon$ of the strain, for the measurement error's standard deviation is

$$s_{meas} \sim \Delta\varepsilon \approx \frac{d\varepsilon}{dr}\cdot\Delta r = \frac{d}{dr}\left(\frac{a}{\sqrt{r}}\right)\cdot\Delta r = -\frac{a}{2r\sqrt{r}}\cdot\Delta r \tag{24}$$

Substituting (24) into the general form of the measurement error's variance (16) and neglecting the first term (constant errors), the model prediction error variance is given by

$$s_r^2 = s_{\text{model}}^2\cdot\varepsilon_r^2 + \left(\frac{a}{2\cdot r\cdot\sqrt{r}}\right)^2\cdot\Delta r^2 \tag{25}$$

where s_{model} and Δr are user selected values.

Near the crack tip ($r\to 0$), the second term in (25) dominates the overall prediction error variance, while far from the crack tip it is the first term in (25) that dominates the prediction error variance. The extend of these regions of domination depend on the value of the ratios $s_{\text{model}}/\Delta r$. Herein, in all results presented, this ratio is selected to be $s_{\text{model}}/\Delta r = 0.5$.

5.3.2 Results of optimal sensor locations and information entropy for Case A

First, the Case A is considered with 2 strain sensors at an optimal location measuring strains ε_x and ε_y. A comparison between two different optimal sensor configurations using 6 sensors is made in Figure 18. The first one (red cross) corresponds to sensors

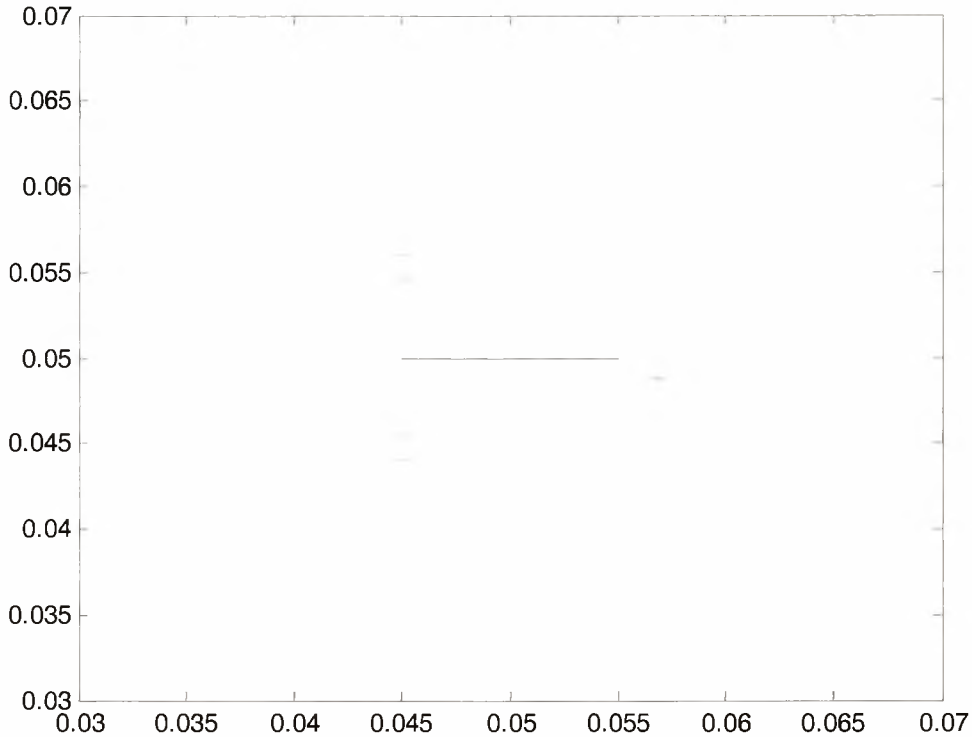

Figure 18: Comparison of 3 optimal sensor locations providing information about the crack parameter set $\underline{\theta} = \{x_0, y_0, a, \phi\}$ and $\underline{\theta} = \{x_0, y_0, a, \phi, \sigma\}$

providing information about the crack parameters set $\underline{\theta} = \{x_0, y_0, a, \phi\}$, while the other one (blue cross) corresponds to sensors providing information about the unknown far field stress as well. As expected, the sensor configuration that provides additional information about the unknown far field stress is in larger distance from the crack tip.

In all results shown next, the optimal sensor configurations correspond to sensors providing information about the crack parameters set $\underline{\theta} = \{x_0, y_0, a, \phi, \sigma\}$. The optimal sensor configurations for Case A are illustrated in Figure 19(a)-(d) for 6, 8, 10, and 12 sensors respectively. These configurations were estimated using the hybrid optimization algorithm for optimizing the information entropy. Comparing the results in Figures 18 and 19(a), it can be clearly seen that, due to symmetry, there are more than one global

solution to the optimal sensor configuration problem. The application of the hybrid optimization algorithm converges to one of the global solutions. Repeating applications of the hybrid optimization algorithm will eventually result in the estimation of all global solutions.

The sequential sensor placement (SSP) algorithm also provides optimal sensor configurations with a minimum computational effort and little loss of information. A comparison between the information entropy of the optimum configurations estimated with the hybrid optimization algorithm and the corresponding ones estimated with the SSP algorithm is shown in Figure 20.

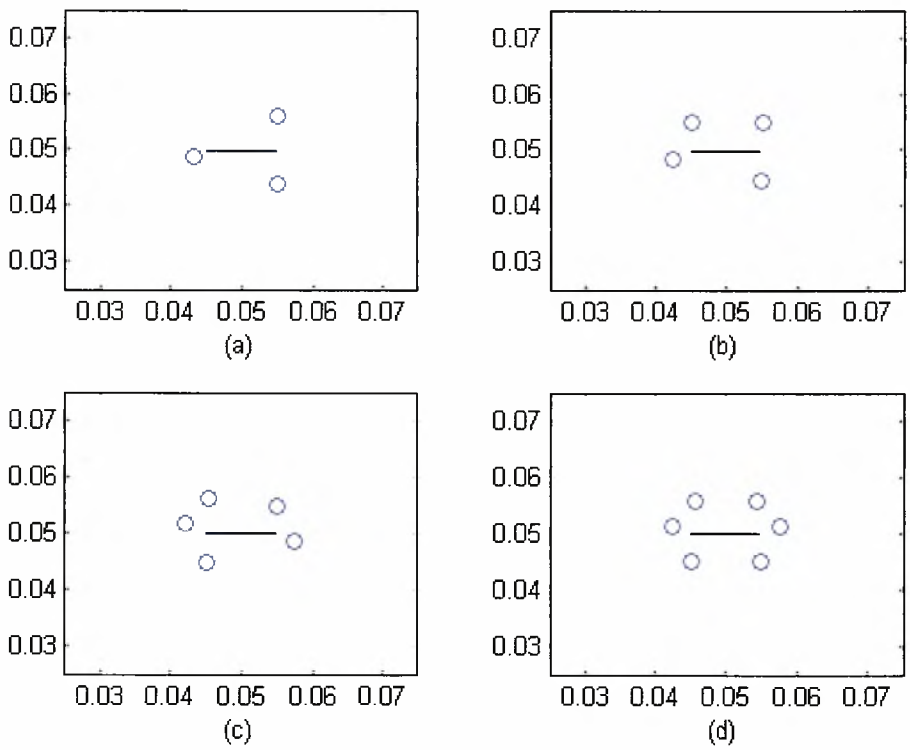

Figure 19: Optimal sensor locations for (a) 6, (b) 8, (c) 10 and (d) 12 sensors.

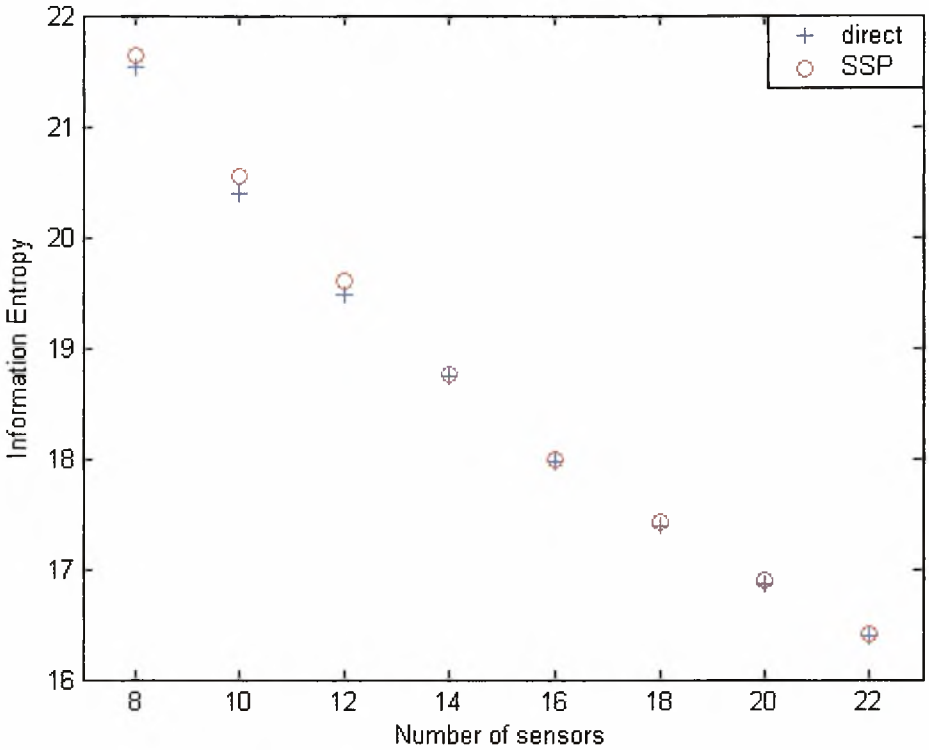

Figure 20: Information entropy-number of sensors for the cases of hybrid optimization and SSP algorithm

Existence of multiple global/local optima

Consider again the estimation of the optimal sensor location of 12 sensors measuring in ε_x and ε_y directions. Let the 5 optimal locations to be known using the direct method and we want to use the SSP algorithm to find the sixth location for the 11^{th} and the 12^{th} sensor. The contour plots of the information entropy as a function of the coordinates x and y of the sensor location is illustrated in Figure 21. It is seen that at least eight local optima exist. The 6^{th} optimal location found with the direct method is shown with the cross. It is clear that the optimization method for estimating the optimal sensor location should be able to identify the global optimum from the local ones. Thus, the proposed optimization algorithm is required to be used since it can locate global optima in the

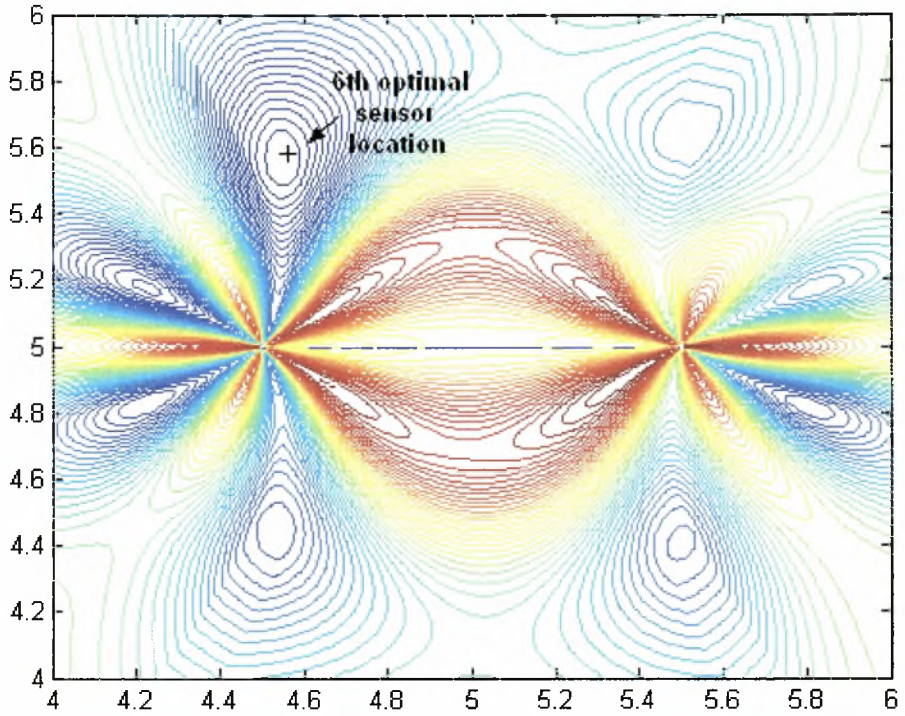

Figure 21: Contour plots of the information entropy as a function of the sensor location

expense of high computational effort. It is worth pointing out that even in the SSP algorithm, the use of the hybrid optimization is necessary. This increases significantly the computational time for estimating the optimal sensor configurations.

Uncertainty in crack parameter estimates

Consider the case of an optimal sensor configuration of 12 sensors for Case A and a corresponding arbitrary grid, as shown in Figure 22. The arbitrary grid is chosen purposely to be closest to the crack. Crack identification results are carried out with these two sensor configurations and the probability distribution $p(\underline{\theta} \mid D)$ of the crack parameters is obtained. Simulated data were generated from a finite element model of a plate with dimension $L = 100a$ and measurement error $n = 2\%$ was added to the

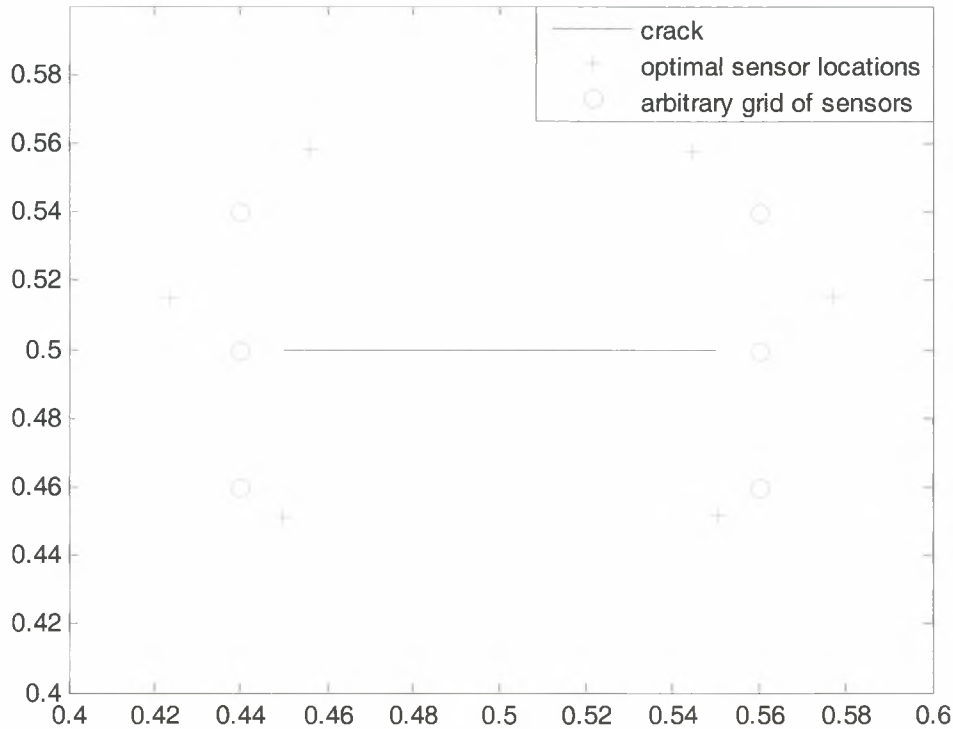

Figure 22: Optimal and arbitrary sensor configurations for the case of 12 sensors

computed strains. Figures 23 and 24 show the contour plots of the probability distribution $p(\underline{\theta} \mid D) / c_1 \pi_\theta(\underline{\theta})$ of the parameter set $\underline{\theta}$ as a function of the crack parameters x_0 and a, holding the rest of the crack parameters y_0, ϕ and stress σ constant. The global optimum is in the area around $x_0 = 0.5$, $a = 0.05$ and corresponds to the chosen values of these parameters in the finite element model that generated the measured data $\hat{\varepsilon}$.

The probability distribution in Figure 24 corresponds to the arbitrary grid of sensors used, while the probability distribution in Figure 23 corresponds to the optimal sensor configuration. It is observed from these figures that in spite of the grid of sensors chosen to be closest to the crack, the use of an optimal sensor configuration resulted in a narrower distribution especially in the direction of x_0 compared to the much wider distribution obtained from the arbitrary grid. This demonstrates that the uncertainty in the

parameter values, quantified by $p(\underline{\theta} | D)$, is less for the optimal configuration than it is for an arbitrary grid of sensors.

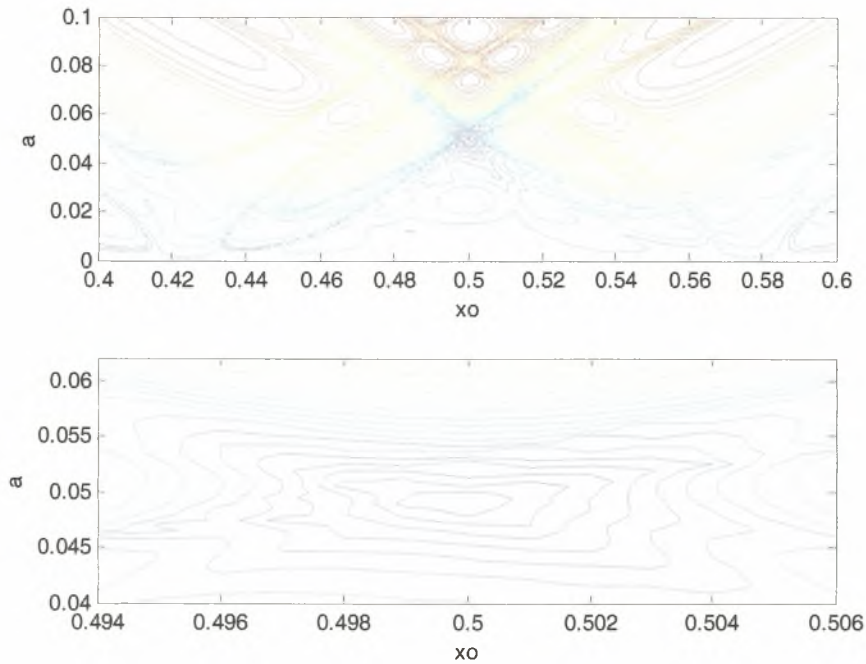

Figure 23: (a) Contour plots of probability distribution as a function of the the crack center x_0 and the crack's half-length a, and (b) zoom in the neighbourhood of the optimum, for the case of optimal sensor configuration

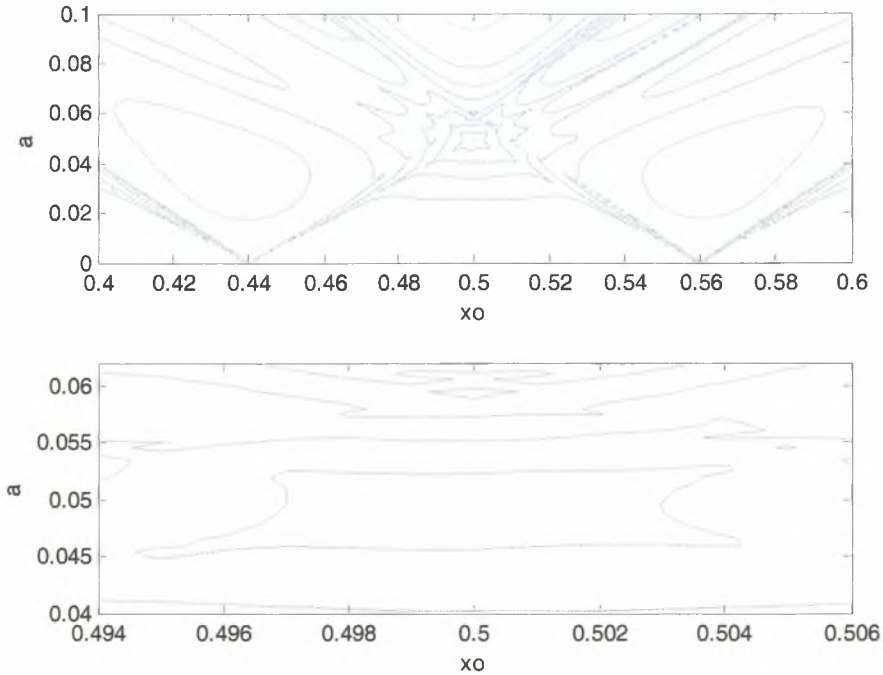

Figure 24: (a) Contour plots of probability distribution as a function of crack center x_0 and the crack's half-length a and (b) zoom in the neighborhood of the optimum, for the case of an arbitrary grid of sensors

5.3.2 Results of optimal sensor configuration and information entropy for Case B

Next, results for the Case B are obtained. The optimal sensor configurations for 6, 8, 10 and 12 sensors are illustrated in Figure 25(a)-(d). In this case the direction in which sensors are placed to measure strains is not prespecified. Instead, it is considered as a variable to be optimized. For this case where the direction β of strain measurements is optimized, the problem of finding the global optima for both sensor location and the measurement angle becomes computationally more difficult. Results showed that the optimal angle of measurement for all sensors is $\beta = 3\pi/2 = 270°$.

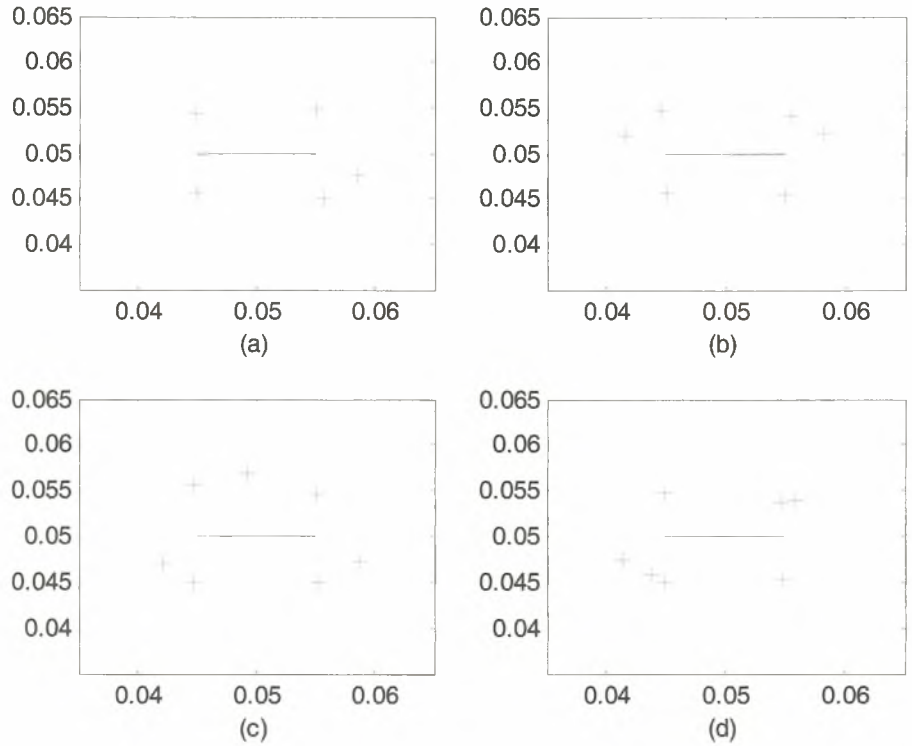

Figure 25: Optimal sensor locations for (a) 5, (b) 6, (c) 7 and (d) 8 sensors. Optimal measurement direction $\beta = 270°$ for all sensors

The minimum values of the information entropy as a function of the number of sensors placed at the optimal location in the structure is shown in Figure 25 for Cases A and B. In case B all sensors placed at optimal locations measure strains in optimal direction $\beta = 270°$. Case B results to configurations with less information entropy, i.e. providing more informative data, for the same number of sensors than case A, as it is shown in Figure 26.

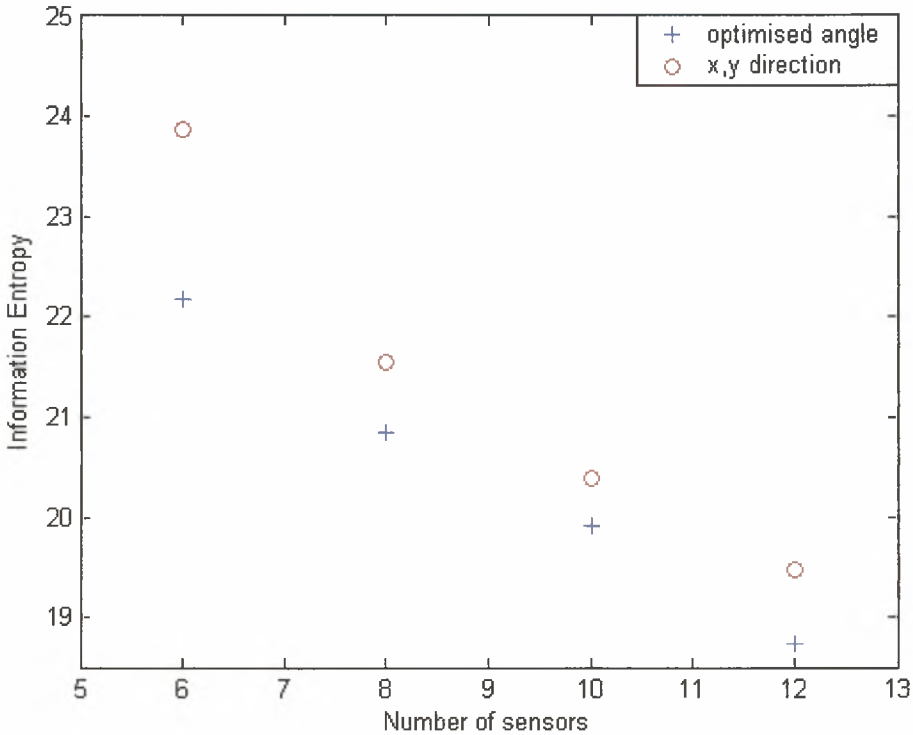

Figure 26: Information entropy-number of sensors for cases A (red) and B (blue)

CHAPTER 6

CONCLUSIONS

A methodology was presented for the estimation of cracks in structures using strain measurements. A Bayesian system identification methodology was used to estimate the location, size and orientation of cracks using the information provided from strain measurements of a cracked thin plate subjected to unknown uniform stress. The analysis showed that the proposed identification methodology can efficiently detect and completely define an existing crack and far field stresses using a simple grid of sensors, even in the presence of measurement and model errors, provided that the model error is sufficiently small.

A parametric analysis was performed with variables (i) the density of the sensor configuration with respect to the crack size, (ii) the distance of cracks center from the central sensor of a uniform 3*x*3 grid of strain sensors with respect to the crack size and (iii) the difference between the crack orientation and the direction of the strain measurements. This analysis provided useful insight about the effect of these variables to the method's accuracy, as well as the limits on which this methodology fails to identify the crack. Results showed that for $\gamma / a < 10$, where γ is characteristic of the sensor grid and a is the half crack length, the methodology can completely identify a crack and the external static load for both cases of strain measurements ε_x, ε_y in each sensor location and that of strain measurements perpendicular to the crack. For the case of strain measurements in a direction parallel to the crack, the values of γ / a for estimating the crack parameters are significantly smaller.

Optimal sensor configurations using the information entropy measure were also derived. A comparison between the case of optimal sensor configurations using sensors measuring strains ε_x and ε_y in an optimal location and the case of configurations with sensors placed at optimal locations measuring strains in an optimal direction β was made. The latter case resulted in configurations that provided more informative data for the same number of sensors than the first case. Results also showed that the optimal measurement direction for all strain sensors, when a crack with orientation $\phi = 0$ is considered, is $\beta = 270°$. This means that most of the information about the crack parameters is derived by strain measurements in a perpendicular direction with respect to the crack, a result also reinforced by the parametric analysis results.

Both optimization problems involved in crack identification and optimal sensor configuration methodologies were proven to have multiple local and global optima. Thus, the use of an effective optimization algorithm is necessary. Evolutionary algorithms are used in order to estimate the neighbourhood of the global optimum, and then the algorithm is switched to a gradient-based optimization algorithm that can converge quickly to the global optimum. The proposed hybrid optimization algorithm is shown to be effective in avoiding local optima and locating the global one. However, in order to find the neighbourhood of the global optimum, evolutionary algorithms require a relatively large number of function evaluations and this makes the proposed approach computationally time consuming.

Despite the computational effort needed and the limitations as far as model and measurement errors are considered, the proposed identification methodology was proven

to be able to detect a crack in a thin plate subject to unknown far field static load that was also estimated, as well as to accurately identify the crack size and orientation.

REFERENCES

[1] A.K. Mal, F. Ricci, S. Banerjee, F. Shih. "A Conceptual Structural Health Monitoring System Based on Vibration and Wave Propagation," *Structural Health Monitoring: An International Journal*, 4(3): 283 - 293 (2005)

[2] M.W. Vanik, J.L. Beck, S.K. Au, "Bayesian probabilistic approach to structural health monitoring", *Journal of Engineering Mechanics* (ASCE) 126 (2000) 738–745.

[3] S.W. Doebling, C.R. Farrar, M.B. Prime, D.W. Shevitz. "Damage identification and health monitoring of structural and mechanical systems from changes in their vibration characteristics: a literature review", Los Alamos National Laboratory Report No. LA-13070- MS, 1996.

[4] S.W. Doebling, C.R. Farrar, M.B. Prime. "A summary review of vibration-based damage identification methods", *The Shock and Vibration Digest* 30 (2) (1998) 91105.

[5] K.D. Hjelmstad, S. Shin. "Crack identification in a cantilever beam from modal response", *Journal of Sound and Vibration* 198 (1996) 527–545.

[6] J.L. Beck, B.S. May, D.C. Polidori. "Determination of modal parameters from ambient vibration data for structural health monitoring", in: Proceedings of the First World Conference on Structural Control, Los Angeles, USA, 1994, pp. 1395–1402.

[7] J.-B. Ihn, F.-K. Chang. "Detection and monitoring of hidden fatigue crack growth using a built-in piezoelectric sensor/actuator network: Part I. Diagnostics," *Smart Materials and Structures*, 2004, Vol. 13, pp. 609-620.

[8] C. Paget, S. Grondel, K. Levin, C. Delebarre. "Damage assessment in composites by Lamb waves and wavelet coefficients", *Smart Materials and Structures 12* (2003) 393–402

[9] V. Giurgiutiou, J. Bao, W. Zhao. "Active Sensor Wave Propagation Health Monitoring of Beam and Plate Structures", *Proceedings of the SPIE's 8th International Symposium on Smart Structures and Materials*, 4-8 March 2001, Newport Beach, CA

[10] B.C. Lee, W.J. Staszewski. "Modeling of Lamb waves for damage detection in metallic structures: Part II. Wave interactions with damage", *Smart Materials and Structures 12* (2003) 815-824

[11] G.J. Tsamasphyros et al., "Selection of Optical Fibers Paths and Sensor Locations for Monitoring the Integrity of Composite Patching", *Applied Composite Materials* 10**:** 331–338, 2003.

[12] G.J. Tsamasphyros et al., "Optimization of Embedded Optical Sensor Location in Composite Repairs", *Applied Composite Materials*, 10**:** 129–140, 2003.

[13] T.E. Munns, A. Bartolini, R.M. Kent et al. 2002. *Health Monitoring for Airframe Structural Characterization*, NASA/CR-2002-211428, Hampton, Virginia, NASA Langley Research Center.

[14] J.L. Beck, "Statistical system identification of structures", in: Proceedings of the 5th International Conference on Structural Safety and Reliability, ASCE, San Francisco, 1989, pp. 1395-1402.

[15] J.L. Beck, L.S. Katafygiotis, "Updating models and their uncertainties—Bayesian statistical framework", American Society of Civil Engineers, *Journal of Engineering Mechanics* 124 (4) (1998) 455–461.

[16] L.S. Katafygiotis, C. Papadimitriou, H.F. Lam, "A Probabilistic Approach to Structural Model Updating", *International Journal of Soil Dynamics and Earthquake Engineering* 17 (7-8) (1998) 495-507.

[17] C. Papadimitriou & L.S. Katafygiotis. 2004. "Bayesian Modeling and Updating Engineering Design Reliability Handbook, E. Nikolaidis, D.M. Ghiocel and S. Singhal (Eds), CRC Press.

[18] L.S. Katafygiotis, H.F. Lam, and C. Papadimitriou (2000). "Treatment of Unidentifiability in Structural Model Updating." *Advances in Structural Engineering- An International Journal*, 3(1), 19-39.

[19] K. Christodoulou & C. Papadimitriou, 2007. "Structural identification based on optimally weighted modal residuals", *Mechanical Systems and Signal Processing, Volume 21, Issue 1, 4-23*

[20] D.C. Kammer, 1991. "Sensor Placements for on Orbit Modal Identification and Correlation of Large Space Structures". *Journal of Guidance, Control and Dynamics,* 14:251-259.

[21] F.E. Udwadia, 1994. "Methodology for Optimal Sensor Locations for Parameter Identification in Dynamic Systems". *Journal of Engineering Mechanics (ASCE)*, 120(2): 368-390.

[22] P.H. Kirkegaard & R. Brincker, 1994. "On the Optimal Locations of Sensors for Parametric Identification of Linear Structural Systems". *Mechanical Systems and Signal Processing*, 8:639-647.

[23] C. Papadimitriou, J.L. Beck & S.K. Au, 2000. "Entropy-Based Optimal Sensor Location for Structural Model Updating". *Journal of Vibration and Control*, 6(5): 781-800.

[24] C. Papadimitriou, 2004. "Optimal Sensor Placement Methodology for Parametric Identification of Structural Systems". *Journal of Sound and Vibration*, 278(4): 923-947.

[25] C. Papadimitriou, 2005. "Pareto Optimal Sensor Locations for Structural Identification". *Computer Methods in Applied Mechanics and Engineering*, 194(12-16): 1655-1673.

[26] N. Bleistein, R. Handelsman, Asymptotic expansions for integrals, Dover, New York, USA, 1986.

[27] C. Papadimitriou, 2002. "Applications of Genetic Algorithms in Structural Health Monitoring". *Proc. 5th World Congress on Computational Mechanics*, (http://wccm.tuwien.ac.at., Vienna, Austria) .

[28] H.G. Beyer, The Theory of Evolution Strategies, Springer, Berlin, 2001.

[29] COMSOL Multiphysics 3.2 User's Guide

[30] D. Broek, "Elementary Engineering Fracture Mechanics", Martinus Nijhoff, The Hague, 1984.

APPENDIX A

WESTERGAARD METHOD FOR STRESS FIELD AROUND CRACK TIPS

(a) Description of the method

The Westergaard semi-inverse method [] constitutes a simple and versatile tool for solving a certain class of plane elasticity problems. It uses the Airy stress function representation, in which the solution of a plane elasticity problem is reduced to finding a function U

$$\nabla^2\nabla^2 U = \frac{\partial^4 U}{\partial x^4} + 2\frac{\partial^4 U}{\partial x^2 \partial y^2} + \frac{\partial^4 U}{\partial y^4} = 0 \tag{1}$$

which satisfies the biharmonic equation and the appropriate boundary conditions.

The stress components are given by

$$\sigma_x = \frac{\partial^2 U}{\partial y^2}, \sigma_y = \frac{\partial^2 U}{\partial x^2}, \tau_{xy} = -\frac{\partial^2 U}{\partial x \partial y}. \tag{2}$$

If we choose the function U in the form

$$U = \psi_1 + x\psi_2 + y\psi_3, \tag{3}$$

where the functions $\psi_i, (i = 1,2,3)$ are harmonic, that is,

$$\nabla^2 \psi_i = \frac{\partial^2 \psi_i}{\partial x^2} + \frac{\partial^2 \psi_i}{\partial y^2} = 0, \tag{4}$$

U will automatically satisfy Equation (1). Following the Cauchy-Riemann conditions for an analytic function of the form

$$Z(z) = \mathrm{Re}\, Z + i\, \mathrm{Im}\, Z \tag{5}$$

where $z = x + iy$, $i = \sqrt{-1}$, and Re and Im denote real and imaginary parts of the function, respectively, we have

$$\mathrm{Re}\frac{dZ}{dz} = \frac{\partial \mathrm{Re}\, Z}{\partial x} = \frac{\partial \mathrm{Im}\, Z}{\partial y}$$

$$\mathrm{Im}\frac{dZ}{dz} = \frac{\partial \mathrm{Im}\, Z}{\partial x} = -\frac{\partial \mathrm{Re}\, Z}{\partial y} \tag{6}$$

and therefore,

$$\nabla^2 \mathrm{Re}\, Z = \nabla^2 \mathrm{Im}\, Z = 0. \tag{7}$$

Thus, the functions the functions $\psi_i, (i = 1, 2, 3)$ in Equation (3) can be considered as the real or imaginary part of an analytic function of the complex variable z. Introducing the notation

$$\bar{\bar{Z}} = \frac{d\bar{\bar{Z}}}{dz},\ Z = \frac{d\bar{Z}}{dz},\ Z' = \frac{dZ}{dz} \tag{8}$$

where bars over Z represent integrations with respect to z, Westergaard defined an Airy function U_I for symmetric problems by

$$U_I = \mathrm{Re}\,\bar{\bar{Z}}_I + y\,\mathrm{Im}\,\bar{Z}_I \tag{9}$$

that automatically satisfies Equation (1). Using Equations (4) we find the stresses from U_I to be

$$\sigma_x = \mathrm{Re}\, Z_I - y\,\mathrm{Im}\, Z_I'$$

$$\sigma_y = \mathrm{Re}\, Z_I + y\,\mathrm{Im}\, Z_I'$$

$$\tau_{xy} = -y\,\mathrm{Re}\, Z_I' \tag{10}$$

(b) Crack problems

Consider a crack of length $2a$ which occupies the segment $-a \le x \le a$ along the x-axis in an infinite plate subjected to uniform equal stresses a along the y and x directions at infinity (Figure 17). If the origin of the coordinate system is defined at the center of the crack, the boundary conditions of the problem may be stated as follows:

$$\sigma_y + i\tau_{xy} = 0 \text{ for } y = 0, \quad -a < x < a \tag{11}$$

and

$$\sigma_x = 0, \ \sigma_y = \sigma, \ \tau_{xy} = 0 \text{ for } \left(x^2+y^2\right)^{1/2} \to \infty \tag{12}$$

The function defined by

$$Z_I = \frac{\sigma z}{\sqrt{z^2 - a^2}}, \tag{13}$$

where σ is the remote stress and a is the half crack length, as defined in Figure 17, satisfies the boundary conditions (11) and (12) and therefore is the Westergaard function for this problem. Note that the imaginary part of the stresses vanishes when $y = 0$. In addition, the shear stress vanishes when $y = 0$, implying that the crack plane is a principal plane. Thus the stresses are symmetric about $\theta = 0$ and Equations (10) imply Mode I loading.

Consider the crack plane where $y = 0$. For $-a < x < a$, Z is pure imaginary, while Z is real for $|x| > |a|$. The normal stresses on the crack plane are given by

$$\sigma_{xx} = \sigma_{yy} = \mathrm{Re}\, Z = \frac{\sigma x}{\sqrt{x^2 - a^2}} \tag{14}$$

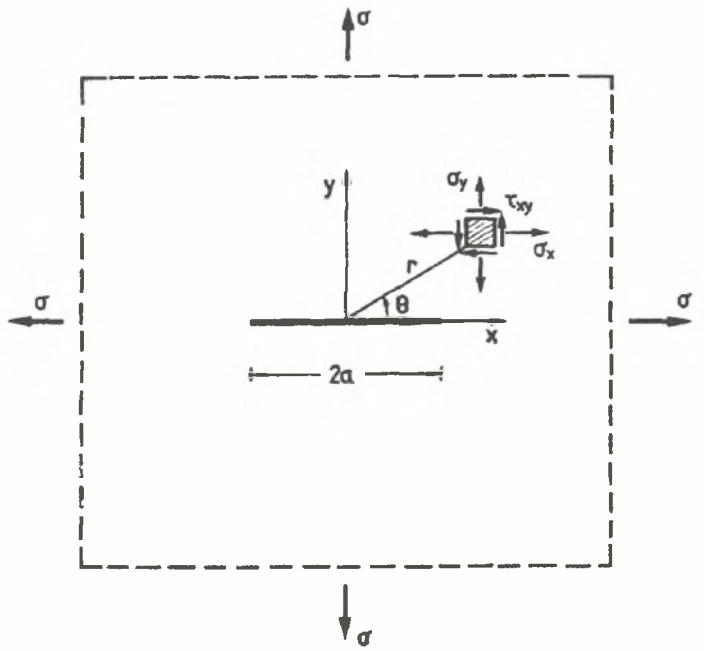

Figure 27. Case of a crack of length 2a in an infinite plate subjected to uniform biaxial tension at infinity

Let us now consider the horizontal plane from each crack tip, $x^* = x - a$; Equation becomes

$$\sigma_{xx} = \sigma_{yy} = \frac{\sigma\sqrt{a}}{\sqrt{2x^*}} \quad \text{for } x^* << a. \tag{15}$$

Thus, the Westergaard approach leads to the expected inverse square-root singularity. One advantage of this analysis is that it relates the local stresses to the global stress and crack size. The Westergaard stress function, in its original form, is suitable for solving a limited range of Mode I crack problems. Subsequent modifications generalized the Westergaard approach to be applicable to a wider range of cracked configurations.

APPENDIX B

FINITE ELEMENT MODELS

All finite element models of the square bounded plate producing the simulated data were created with COMSOL Multiphysics 3.2. In Figure 28 the model with dimensions $L = 100a$ is shown near the area of the crack. The plate was meshed with a large number of finite elements near the crack area and fewer elements at far field as shown in Figure 28. The dimensions were chosen so as to obtain a minimum model error since the solution providing the model predictions was for a plate of infinite dimensions. In order to examine the efficiency of the method with larger model error a plate with smaller dimensions $L = 10a$ (Fig. 29) was used to produce the simulated data of strain measurements. Plots of the normal stresses s_x in front of the crack tip are shown in Figure 30 for the analytical solution and the two computational models.

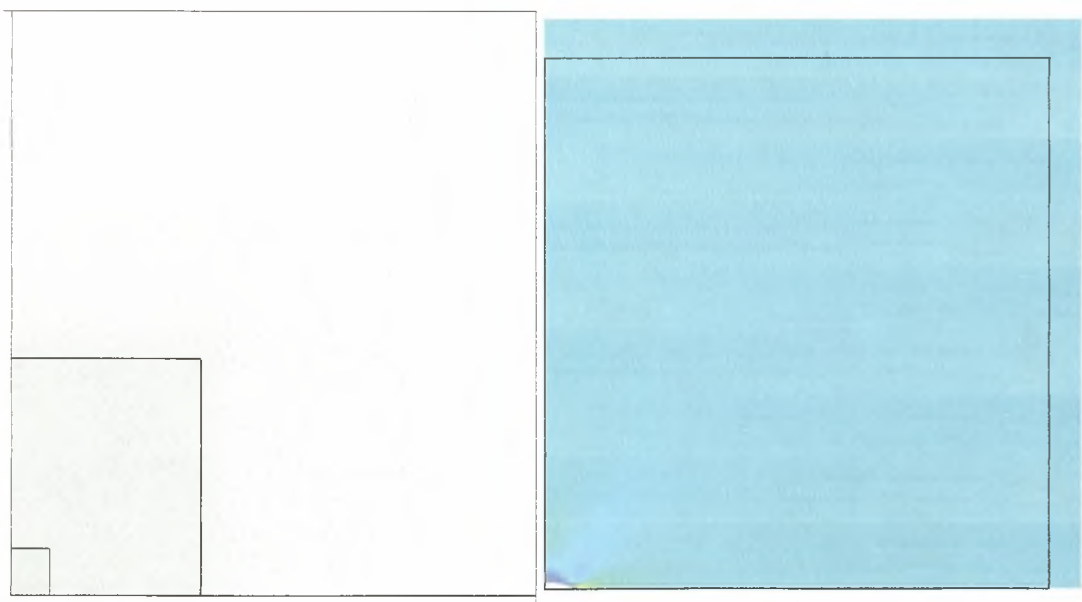

Figure 28. Finite element mesh of the plate (one quarter) with dimensions $100a \cdot 100a$ near the region of the crack

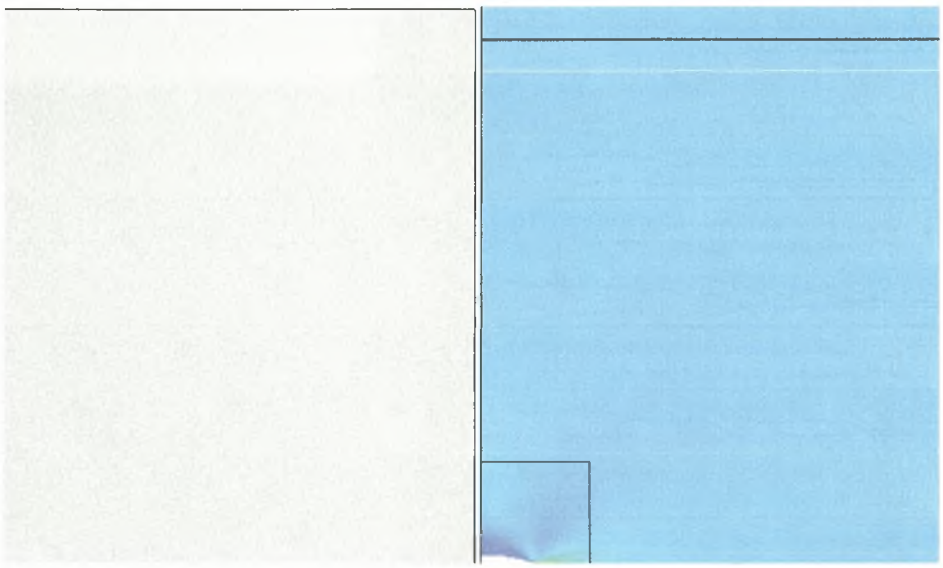

Figure 29. Finite element mesh of the plate (one quarter) with dimensions $10a \cdot 10a$

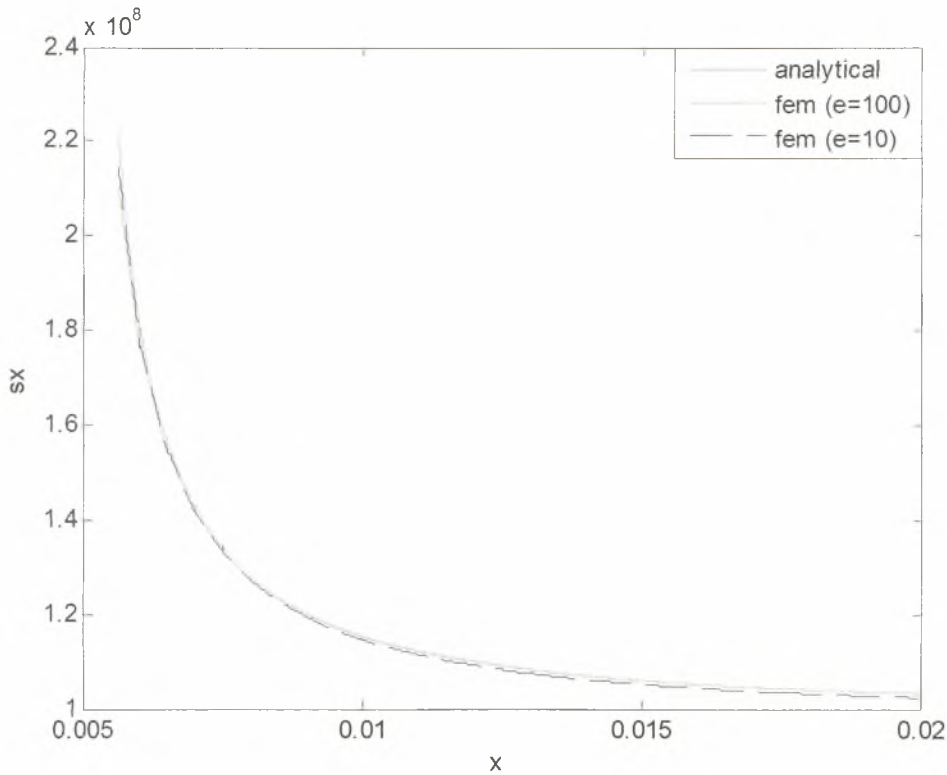

Figure 30. Normal stress s_x as a function of x in front of the crack-tip